Recombinant rotaviruses rescued by reverse genetics reveal the role of NSP5 hyperphosphorylation in the assembly of viral factories

Guido Papa[1,*], Luca Venditti[1], Francesca Arnoldi[1,2], Elisabeth M. Schraner[3], Christiaan Potgieter[4,5], Alexander Borodavka[6], Catherine Eichwald[3] and Oscar R. Burrone[1,*]

[1] International Centre for Genetic Engineering and Biotechnology, ICGEB, Padriciano 99, 34149 Trieste, Italy
[2] Department of Medicine, Surgery and Health Sciences, University of Trieste, Trieste, Italy
[3] Institute of Virology, University of Zürich, Zürich, Switzerland
[4] Department of Biochemistry, Centre for Human Metabolomics, North-West University, Potchefstroom, South Africa
[5] Deltamune (Pty) Ltd, 248 Jean Avenue, Lyttelton, Centurion, South Africa
[6] Astbury Centre for Structural Molecular Biology, School of Molecular and Cellular Biology, University of Leeds, Leeds, UK

* Corresponding authors, guido.papa@icgeb.org, burrone@icgeb.org

ABSTRACT

Rotavirus (RV) is a non-enveloped RNA virus that replicates in round-shaped cytoplasmic viral factories termed viroplasms. The formation of these viral factories requires the co-expression of the two non-structural viral proteins NSP5 and NSP2.

During RV infection, NSP5 undergoes hyperphosphorylation, which is primed by the phosphorylation of a single serine residue. Despite extensive phosphorylation, the role of this post-translational modification in the formation of viroplasms and its impact on the virus replication remains obscure. Here we shed light on the role of NSP5 during RV infection by taking advantage of a modified fully tractable reverse genetics system. An NSP5 trans-complementing cell line was used to generate and characterise several recombinant rotaviruses (rRVs) with mutations in NSP5. We demonstrate that a rRV lacking NSP5, was completely unable to assemble viroplasms and to replicate, confirming its pivotal role in rotavirus replication.

A number of mutants with impaired NSP5 phosphorylation were generated to further interrogate the function of this post-translational modification in the assembly of replication-competent viroplasms. We showed that the rRV mutant strains exhibit impaired viral replication and the ability to assemble round-shaped viroplasms in MA104 cells. Furthermore, we have investigated the mechanism of NSP5 hyper-phosphorylation during RV infection using NSP5 phosphorylation-negative rRV strains, as well as MA104-derived stable transfectant cell lines expressing either wt NSP5 or selected NSP5 deletion mutants. Our results indicate that NSP5 hyper-phosphorylation is a crucial step for the assembly of round-shaped viroplasms, highlighting the key role of the C-terminal tail of NSP5 in the formation of replication-competent viral factories. Such a complex NSP5 phosphorylation cascade may serve as a paradigm for the assembly of functional viral factories in other RNA viruses.

AUTHOR SUMMARY

Rotavirus (RV) is considered the most common cause of viral gastroenteritis in children worldwide. RV double-stranded RNA genome is replicated and packaged into virus progeny in cytoplasmic structures termed viroplasms. The non-structural protein NSP5, which undergoes a complex hyperphosphorylation process during RV infection, is required for the formation of these virus-induced organelles. However, its roles in viroplasm formation and RV replication have never been directly assessed due to the lack of a fully tractable reverse genetics (RG) system for rotaviruses.

Here we show a novel application of a recently developed RG system by establishing a stable trans-complementing NSP5-producing cell line required to rescue rotaviruses with mutations in NSP5. This approach allowed us to provide the first direct evidence of the pivotal role of this protein during RV replication. Furthermore, using recombinant RV mutants we shed light on the molecular mechanism of NSP5 hyperphosphorylation during infection and its involvement in the assembly and maturation of replication-competent viroplasms.

Considering that hyperphosphorylation of proteins appears to be a common mechanism regulating many cellular processes, our work suggests a key role of these multiple phosphorylation events in orchestrating assembly of structures required for replication of other virus pathogens.

INTRODUCTION

Rotavirus (RV) is the most common cause of viral gastroenteritis in young children and infants worldwide [1,2]. It is a non-enveloped RNA virus with a genome composed of 11 segments of double-stranded RNA (dsRNA), which replicates in cytoplasmic structures primarily composed of viral proteins [3–5]. During infection, the first steps of viral morphogenesis and genome replication occur within cytoplasmic viral replication factories known as viroplasms. [3,5–7]. The assembly of viroplasms requires co-expression of at least two non-structural proteins, NSP5 and NSP2 [8,9], however, how these virus-induced organelles are formed remains unknown.

Other viral proteins also found in viroplasms include RNA-dependent RNA polymerase (RdRp) VP1, the main inner-core protein VP2, guanyltransferase/ methylase VP3, and the middle layer (inner capsid) protein VP6 [10,11]. Biochemical evidence suggests that viroplasms are essential for RV replication since the virus production is highly impaired upon silencing of either NSP2 or NSP5 [12–15].

Rotavirus NSP5, encoded by genome segment 11, is a small serine (Ser)- and threonine (Thr)-rich non-structural protein that undergoes multiple post-translational modifications in virus-infected cells, including O-linked glycosylation [16], N-acetylation [17], SUMOylation [18] and crucially hyperphosphorylation that involves several distinct Ser residues [19,20]. The NSP5 hyperphosphorylation is a complex process, which gives rise to multiple phosphorylation states ranging from the most abundant 28 kDa phospho-isoform, up to the hyperphosphorylated 32-34 kDa states [19,20]. All these forms have been found to be more stable in viroplasms, while chemical disruption of viroplasms results in NSP5 de-phosphorylation [21]. The mechanism of NSP5 phosphorylation is not yet wholly understood, but it involves interactions with other viral proteins. When expressed alone in non-infected cells, NSP5 is not phosphorylated, while co-expression with NSP2 or VP2 results in NSP5 hyperphosphorylation and formation of viroplasm-like structures (VLS) [8,22,23]. NSP5 hyperphosphorylation involves the phosphorylation of Serine 67 (Ser67) by

128 Casein Kinase 1α (CK1α) to initiate the phosphorylation cascade [24,25] and it is
129 considered to be essential for the assembly of viroplasms [26].
130 Although the structure of NSP5 remains unknown, it readily forms higher
131 molecular weight oligomeric species in solution, potentially providing a larger
132 interface for interacting with multiple components of viroplasms [27].
133 In addition, the C-terminal region ('a tail' including amino acids 180-198) is
134 required for NSP5 decamerisation *in vitro* [27] and VLS formation *in vivo* [7].
135 However, due to the lack of a fully tractable reverse genetics (RG) system for
136 RVs until recently, previous studies on NSP5 have been carried out using the
137 mutants expressed in the absence of a complete set of viral proteins. Here, we
138 took advantage of the novel plasmid only-based, helper-virus free RG systems
139 for rotaviruses [28,29] to gain new insights into the mechanisms of NSP5
140 hyperphosphorylation and its role in viroplasm assembly and virus replication
141 during viral infection.
142 To achieve this, we generated and characterised several viable recombinant
143 rotaviruses (rRVs) with mutations in NSP5. Using these mutants, we show the
144 essential role of NSP5 hyperphosphorylation for viroplasm assembly and in
145 genome replication. These studies shed light on a complex hierarchical
146 mechanism of NSP5 hyperphosphorylation during rotaviral infection.
147
148 **MATERIALS AND METHODS**
149
150 **Cells and viruses**. MA104 (embryonic African green monkey kidney cells,
151 ATCC® CRL-2378), U2OS (Human bone osteosarcoma epithelial cells), Caco-2
152 (colorectal adenocarcinoma human intestinal epithelial cell line, ATCC®HTB-37)
153 and HEK293T (embryonic human kidney epithelial, ATCC®CRL-3216) cells were
154 cultured in Dulbecco's Modified Eagle's Medium (DMEM) (Life Technologies)
155 supplemented with 10% Fetal Bovine Serum (FBS) (Life Technologies) and 50
156 µg/ml gentamycin (Biochrom AG).

157 MA104-NSP5-EGFP cells (MA-NSP5-EGFP) [7] were cultured in DMEM
158 supplemented with 10% FBS (Life Technologies), 50 µg/ml gentamycin
159 (Biochrom AG) and 1 mg/ml geneticin (Gibco-BRL, Life Technologies).
160 MA104-NSP2-mCherry (MA-NSP2-mCherry), MA104-Δ3 (MA-Δ3), MA104-Δtail
161 (MA-ΔT) and MA104-NSP5wt (MA-NSP5) stable transfectant cell lines
162 (embryonic African green monkey kidney cells, ATCC® CRL-2378) were grown
163 in DMEM (Life Technologies) containing 10% FBS, 50 µg/ml gentamycin
164 (Biochrom AG) and 5 µg/ml puromycin (Sigma-Aldrich).
165 BHK-T7 cells (Baby hamster kidney stably expressing T7 RNA polymerase) were
166 cultured in Glasgow medium supplemented with 5% FBS, 10% Tryptose
167 Phosphate Broth (TPB) (Sigma-Aldrich), 50 µg/ml gentamycin (Biochrom AG),
168 2% Non-Essential Amino Acid (NEAA), 1% Glutamine.
169 Recombinant simian RV strain SA11 (rRV-wt), rescued using reverse genetics
170 system using cDNA clones encoding the wild-type SA11 (G3P[2]) virus [28], was
171 propagated in MA104 cells cultured in DMEM supplemented with 0.5 µg/ml
172 trypsin (Sigma Aldrich).
173
174 **Recombinant RVs Titration**
175 Recombinant NSP5 mutant RVs were grown in MA-NSP5 cells and the lysate
176 was 2-fold serially diluted and used to infect MA-NSP5 cells, seeded in 24-wells
177 plates with coverslips. After 1 hour of adsorption, virus was removed, and cells
178 were incubated at 37°C. At 5 hours post-infection (hpi), cells were fixed with 4%
179 paraformaldehyde (PFA) in phosphate buffer saline (PBS) [137 mM NaCl; 2.7
180 mM KCl; 8.1 mM Na_2HPO_4 and 1.74 mM KH_2PO_4 pH7.5] for 15 min at room
181 temperature and permeabilized for 5 min with PBS containing 0.01% Triton X-
182 100. Next, cells were incubated for 30 min with PBS supplemented with 1%
183 bovine serum albumin (PBS-BSA) at room temperature and then with anti-NSP5
184 (1:1000) or anti-VP2 (1:200) or anti-NSP2 (1:200) guinea pig serum diluted in
185 PBS-BSA. After washing three times with PBS, cells were incubated for 1 h at
186 room temperature with TRITC-conjugated Anti-guinea Pig IgG (Jackson
187 ImmunoResearch) (1:500) diluted in PBS-BSA.

188 Nuclei were stained with ProLong™ Diamond Antifade Mountant with DAPI
189 (Thermo Scientifc). Samples were imaged using a confocal setup (Zeiss Airyscan
190 equipped with a 63x, NA=1.3 objective). Each viroplasms-containing cell was
191 counted as one focus-forming unit (FFU). The average of cells with viroplasms of
192 six fields of view per each virus dilution was determined and the total number of
193 cells containing viroplasms in the whole preparation was estimated. The virus
194 titre was determined as:

195 $$Virus\ Titer\ \left(\frac{FFU}{ml}\right) = \frac{N * Dilution\ Factor}{V(ml)}$$

196 where *N* is a total number of cells containing 1 or more viroplasms, and *V* is the
197 volume of virus inoculum added.
198
199 **Replication Kinetics of recombinant viruses**
200 MA104 cell line (ATCC CRL-2378.1) or stably transfected MA104 cells (NSP5;
201 Δ3, ΔT) were seeded into 24-well plates and subsequently infected with
202 recombinant RVs at MOI (FFU/cell) of 0.5 for multi-step growth curve
203 experiments and MOI 5 for a single-step growth curve experiment. After
204 adsorption for 1 h at 37°C, cells were washed twice with PBS and the medium
205 replaced with DMEM without trypsin. After incubation at 37°C, cells were
206 harvested after 8, 16, 24, 36 hours post virus adsorption. The cell lysates were
207 freeze-thawed three times and activated with trypsin (1 μg/ml) for 30 min at 37°C.
208 The lysates were used to infect monolayers of MA-NSP5 cells seeded in μ-Slide
209 8 Well Chamber Slide-well (iBidi GmbH, Munich, Germany). The cells were then
210 fixed 5 hours post infection for 15 min with 4% paraformaldehyde and
211 permeabilized for 5 min with PBS containing 0.01% Triton X-100. Next, cells
212 were incubated for 30 min with PBS-BSA at room temperature and then with anti-
213 NSP5 serum (1:1000) diluted in PBS-BSA. After three washes with PBS, cells
214 were incubated for 1 h at room temperature with TRITC-conjugated Anti-guinea
215 Pig IgG (Jackson ImmunoResearch) (1:500) diluted in PBS containing 1% BSA
216 (PBS-BSA).

217 The number of infected cells was counted, and the virus titres were expressed in
218 Focus-Forming Units per mL (FFU/mL).
219
220 **Plasmid construction.**
221 RV plasmids pT_7-VP1-SA11, pT_7-VP2-SA11, pT_7-VP3-SA11, pT_7-VP4-SA11,
222 pT_7-VP6-SA11, pT_7-VP7-SA11, pT_7-NSP1-SA11, pT_7-NSP2-SA11, pT_7-NSP3-
223 SA11, pT_7-NSP4-SA11, and pT_7-NSP5-SA11 [28] were used to rescue
224 recombinant RVs by reverse genetics. pT_7-NSP5/S67A carrying a mutation in the
225 nucleotide T220G in the gs11 and pT_7-NSP5/Tyr18Stop harbouring a nucleotide
226 substitution T75G were generated by QuikChange II Site-Directed Mutagenesis
227 (Agilent Technologies). pT_7-NSP5/ΔT was generated from pT_7-NSP5-SA11 by
228 deleting the last 18 C-terminal amino acids (FALRMRMKQVAMQLIEDL) using
229 substitution of the F181 encoding triplet with a stop codon. pT_7-NSP5/Δ176-180
230 were obtained deleting the amino acids 176 to 180 (YKKKY). The described
231 deletions were performed using the QuikChange II Site-Directed Mutagenesis kit
232 (Agilent Technologies).
233 For the generation of lentiviral plasmids, NSP5 and NSP2-mCherry were
234 amplified by PCR and inserted into the plasmid pAIP (Addgene #74171; [30] at
235 the *NotI-EcoRI* restriction enzymes sites to yield pAIP-NSP5 and pAIP-NSP2-
236 mCherry, which were then used to generate lentiviruses for the MA104-stable
237 transfectant cell lines (MA-NSP5 and MA-NSP2-mCherry) [31]. NSP5/ΔT was
238 amplified from the pT_7-NSP5/ΔT by PCR and inserted into the pPB-MCS (Vector
239 Builder) at restriction enzyme sites *NheI-BamHI* to generate pPB-NSP5/ΔT for
240 the production of the stable transfectant MA-ΔT.
241 pPB-NSP5/Δ3, for MA-Δ3 stable cell line establishment, was generated with a
242 GenParts™ DNA Fragment (GenScript) containing NSP5 ORF lacking the amino
243 acids 80-130 (VKTNADAGVSMDSSAQSRPSSNVGCDQVDFSLNKG
244 LKVKANLDSSISIST) and inserted into the *Nhe*I-*BamH*I restriction sites of pPB-
245 MCS vector.
246
247 **Generation of stable cell lines**

248 MA-NSP5-EGFP were generated as previously described [7].
249 MA-NSP2-mCherry and MA-NSP5 cell line were generated using lentiviral vector
250 system [31]. Briefly, HEK293T cells were maintained in DMEM (Life
251 Technologies) supplemented with 10% FBS (Life Technologies), and 50 µg/ml
252 gentamycin (Biochrom AG). Approximately 7 × 10^6 HEK293T cells were seeded
253 in 10 cm^2 tissue culture dishes 24 hours before transfection. For each well, 2.4
254 µg of pMD2-VSV-G, 4 µg of pMDLg pRRE, 1.8 µg of pRSV-Rev and 1.5 µg of
255 plasmid containing pAIP-NSP2-mCherry or pAIP-NSP5 and the human
256 immunodeficiency virus long terminal repeats were co-transfected with
257 Lipofectamine 3000 (Sigma-Aldrich) according to the manufacturer's instructions.
258 After 48 h, the virus was collected by filtration with a 0.45-µm polyvinylidene
259 fluoride filter and was immediately used or stored at −80 °C. For lentiviral
260 transduction, MA104 cells were transduced in six-well plates with 1 ml of lentiviral
261 supernatant for 2 days.
262 MA-Δ3 and MA-ΔT were generated using the PiggyBac Technology [32]. Briefly,
263 10^5 MA104 cells were transfected with the pCMV-HyPBase [32] and the
264 transposon plasmid pPB-NSP5/Δ3 and pPB-NSP5/ΔT using a ratio of 1:2.5 with
265 Lipofectamine 3000 (Sigma-Aldrich) according to the manufacturer's instructions.
266 The cells were maintained in DMEM supplemented with 10% FBS for 3 days and
267 then the cells were incubated with DMEM supplemented with 10% FBS and 5
268 µg/ml puromycin (Sigma-Aldrich) for 4 days to allow the selection of cells
269 expressing the gene of interest.
270
271 **Rescue of recombinant RVs (rRVs) from cloned cDNAs.**
272 To rescue recombinant RV strain SA11 (rRV-WT), monolayers of BHK-T7 cells
273 (4 × 10^5) cultured in 12-well plates were co-transfected using 2.5 µL of TransIT-
274 LT1 transfection reagent (Mirus) per microgram of DNA plasmid. Each mixture
275 comprised 0.8 µg of SA11 rescue plasmids: pT_7-VP1, pT_7-VP2, pT_7-VP3, pT_7-
276 VP4, pT_7-VP6, pT_7-VP7, pT_7-NSP1, pT_7-NSP3, pT_7-NSP4, and 2.4 µg of pT_7-
277 NSP2 and pT_7-NSP5 (Komoto et. al, 2018). Furthermore 0.8 µg of pcDNA3-

278 NSP2 and 0.8 µg of pcDNA3-NSP5, encoding NSP2 and NSP5 proteins, were
279 also co-transfected to increase rescue efficiency.
280 To rescue recombinant rRVs encoding NSP5 mutants, pT_7 plasmids encoding
281 NSP5/S67A, NSP5/Y18Stop, NSP5/Δ180-198 segments were used instead of
282 pT_7-NSP5. At 24 h post-transfection, MA-NSP5 cells (5×10^4 cells) were added
283 to transfected cells to provide a functional NSP5 for the virus rescue. The cells
284 were co-cultured for 3 days in FBS-free medium supplemented with trypsin (0.5
285 µg/mL) (Sigma Aldrich). After incubation, transfected cells were lysed by freeze-
286 thawing and 200 µl of the lysate was transferred to fresh MA-NSP5 cells. After
287 adsorption at 37°C for 1 hour, cells were washed three times with PBS and
288 further cultured at 37°C for 4 days in FBS-free DMEM supplemented with 0.5
289 µg/mL trypsin (Sigma Aldrich, 9002-07-7) until a clear cytopathic effect was
290 visible. The recombinant viruses were then checked by RT-PCR.
291
292 **Immunofluorescence microscopy**
293 Immunofluorescence experiments were performed using µ-Slide 8 Well Chamber
294 Slide-well (iBidi GmbH, Munich, Germany) and the following antibody dilutions:
295 anti-NSP5 guinea pig serum 1:1,000; anti-NSP2 guinea pig serum 1:200; anti-
296 VP2 guinea pig serum 1:500; anti-VP6 mouse monoclonal antibody 1:1,000;
297 Alexa Fluor 488-conjugated anti-mouse, 1:500 (Life Technologies), and TRITC-
298 conjugated anti-guinea pig, 1:500 (Life Technologies).
299
300 **5-Ethynyl-Uridine (EU) labeling**
301 Newly synthesized RNAs were labeled by including 2 mM 5-ethynyl uridine (EU)
302 into the cell culture medium, and modified incorporated nucleotides were reacted
303 with an azide-conjugated fluorophore Alexa-488 following the manufacturer's
304 protocol for Click-iT RNA Alexa Fluor 488 imaging kit (Thermo Fisher Scientific).
305 Cell nuclei were stained with ProLong™ Diamond Antifade Mountant with 4',6-
306 diamidino-2-phenylindole (DAPI, Thermo Scientific). Samples were imaged using
307 a confocal setup (Zeiss Airyscan equipped with a 63x, NA=1.3 objective), and the
308 images were processed using ZEN lite software.

309

310 **RNA Fluorescence in situ Hybridization (FISH)**

311 Rotavirus-infected MA104 cells were fixed with 4% (v/v) paraformaldehyde in
312 nuclease-free Dulbecco's phosphate saline buffer (DPBS) for 10 min at room
313 temperature. Samples were washed twice with DPBS, and then permeabilized
314 with 70% (v/v) ethanol in RNAse-free water at +4ºC for at least 1 hour prior to
315 hybridization. Permeabilized samples were re-hydrated for 5 min in a pre-
316 hybridization buffer (300 mM NaCl, 30 mM trisodium citrate, pH 7.0 in nuclease-
317 free water, 10 % v/v formamide, supplemented with 2 mM vanadyl ribonucleoside
318 complex). Re-hydrated samples were hybridized with 62.5 nM of an equimolar
319 mixture of Cy3-labelled DNA probes designed to target the coding region of the
320 gene segment 6 of simian rotavirus A/SA11 (Genbank Acc. AY187029.1) using
321 Stellaris Probe Designer v2 software (LCG Biosearch Technologies), in a total
322 volume of 200 µl of the hybridization buffer (Stellaris RNA FISH hybridization
323 buffer, SMF-HB1-10, Biosearch Technologies, supplemented with 10% v/v of
324 deionized formamide). After 4-8 hours of incubation at 37°C in a humidified
325 chamber, samples were briefly rinsed with the wash buffer (300 mM NaCl, 30
326 mM trisodium citrate, pH 7.0, 10 % v/v formamide in nuclease-free water), after
327 which a fresh aliquot of 300 µl of the wash buffer was applied to each sample
328 and incubated twice at 37°C for 30 min. After 2 washes, nuclei were briefly
329 stained with 300 nM DAPI solution in 300 mM NaCl, 30 mM trisodium citrate, pH
330 7.0, and the samples were finally rinsed with and stored in the same buffer
331 without DAPI prior to imaging.

332

333 **Transmission electron microscopy.** MA104 cells were seeded at $1x10^5$ cells in
334 2 cm^2 wells onto sapphire discs and infected at MOI of 75 FFU/cell. At 10 hpi,
335 cells were fixed with 2.5% glutaraldehyde in 100 mM Na/K phosphate buffer, pH
336 7.4 for 1 h at 4˚C and kept in that buffer overnight at 4˚C. Afterward, samples
337 were postfixed with 1% osmium tetroxide in 100 mM Na/K phosphate buffer for
338 1h at 4˚C and dehydrated in a graded ethanol series starting at 70%, followed by
339 two changes in acetone, and embedded in Epon. Ultrathin sections (60 to 80 nm)

340 were cut and stained with uranyl acetate and lead citrate [33]. Samples were
341 analysed in a transmission electron microscope (CM12; Philips, Eindhoven, The
342 Netherlands) equipped with a charge-coupled-device (CCD) camera (Ultrascan
343 1000; Gatan, Pleasanton, CA, USA) at an acceleration of 100 kV.
344
345 **λ-Protein phosphatase and Calf Intestinal Alkaline Phosphatase Assays**
346 Cellular extracts were incubated with 2,000 units of λ-protein phosphatase (λ-
347 Ppase) (New England Biolabs) in 50 mM Tris-HCl (pH 7.5), 0.1 mM EDTA, 5 mM
348 DTT, 0.01% Brij 35, and 2 mM $MnCl_2$. The mixture was incubated at 30°C for 2 h.
349 Samples were loaded in SDS-PAGE and analysed by Western blotting.
350 For the Calf Intestinal Alkaline Ppase (CIP) assay, cellular extracts were
351 incubated with 1,000 units of CIP (New England Biolabs) in CutSmart™ reaction
352 buffer (New England Biolabs) and incubated at 30°C for 2h. Samples were
353 subjected to SDS-PAGE and analysed by Western blotting.
354
355 **Electrophoresis of Viral dsRNA Genomes.**
356 Viral dsRNA was extracted with RnaZol® (Sigma-Aldrich) according the
357 manufacturer's protocol. Viral dsRNA genome segments from rRVs-infected cells
358 was mixed with Gel Loading Dye, Purple (6X) (New England Biolabs). The
359 dsRNAs segments were resolved on 10% (wt/vol) poly-acrylamide gels (PAGE)
360 for 2 hours at 180 Volts and visualized by ethidium bromide staining (1μg/ml).
361
362 **Protein Analysis**
363 Proteins derived from rRVs-infected cellular extract were separated on an SDS-
364 PAGE for 2 hours at 35 mA and transferred to polyvinylidene difluoride
365 membranes (Millipore; IPVH00010) for 1 hour and 30 minutes at 300 mA [24].
366 For protein analysis membranes were incubated with the following primary
367 antibodies: anti-NSP5 (1:5,000) [16], anti-VP2 (1:5,000) [10], anti-NSP2 guinea
368 pig sera (1:2,000). The membranes were then incubated with the corresponding
369 horseradish peroxidase (HRP)-conjugated goat anti-guinea pig (1:10,000;

370 Jackson ImmunoResearch). Mouse HRP-conjugated anti-actin mAb (1:35,000)
371 (clone AC-15, Sigma-Aldrich) was used as loading control.
372 Signals were detected using the enhanced chemiluminescence system (Pierce
373 ECL Western blotting substrate; Thermo Scientific).
374
375 **Statistics used**
376 Statistical analysis and plotting were performed using GraphPad Prism 6
377 software (GraphPad Prism 6.0, GraphPad Software Inc., La Jolla, CA, USA).
378 Error bars represent standard deviation. Data were considered to be statistically
379 significant when $p < 0.05$ by Student's t test.
380
381 **RESULTS**
382 **Generation of gs11 mutated recombinant RVs**
383 Recombinant rotaviruses (simian rotavirus A strain SA11) carrying different
384 mutations in the NSP5 coding region of gs11 were obtained using a recently
385 developed reverse genetics protocol [29]. Two essential modifications were
386 introduced to *trans*-complement the potential loss of NSP5 function in the rRV
387 mutants: i) an additional T7-driven plasmid encoding the ORF of wt NSP5 (i.e.,
388 without gs11 5' and 3' UTRs) was included in the transfection step of BHK-T7
389 cells; and ii) each rescued rRV was amplified in a stable transfectant cell line MA-
390 NSP5, supplying the wt NSP5 in trans (Fig. S1). Crucially, we established MA-
391 NSP5 cell line to support the replication of NSP5-deficient recombinant viruses to
392 enable their further in-depth characterisation. These mutants, as well as
393 additional stable cell lines generated for this study as described in Materials and
394 Methods, are summarised in Fig. S2 and S3A-B.
395
396 **<u>rRV-NSP5/KO</u>**
397 NSP5 expression and localisation to viroplasms in virus-infected cells have been
398 considered essential for virus replication [12,13,25,34]. Previous studies, using
399 siRNA targeting gs11 mRNA have shown strong impairment of RV replication
400 [12,13]. We, therefore, established MA104 cell line stably expressing NSP5 to

401 supply NSP5 in trans in order to investigate the effect of point mutations and
402 deletions within the NSP5 gene. In addition, we also made two cell lines
403 expressing NSP2-mCherry and NSP5-EGFP fusions, which are rapidly and
404 efficiently recruited into viroplasms upon virus infection (Fig. S2) [7,22].
405 Here we provide direct demonstration of the essential role of NSP5 in RV
406 replication, using an NSP5 knock out rRV (termed rRV-NSP5/KO) generated by
407 reverse genetics. To rescue the NSP5/KO strain a premature stop codon at the
408 position 18 (Tyr18Stop) was introduced within the NSP5-coding mRNA (Fig.
409 S3A-B). Analysis of MA104-virus-infected cell extracts confirmed the presence of
410 NSP2 and VP2, but not of NSP5 (Fig. 1A). Moreover, we did not detect
411 viroplasms containing NSP2, VP2 or VP6 in both MA104-infected cells and in
412 stable transfectant cell lines expressing the fluorescent fusion proteins NSP2-
413 mCherry or NSP5-EGFP (Fig. S2 and Fig. 1B). Furthermore, both genomic
414 dsRNA synthesis and infectious progeny virus production were completely
415 abrogated in MA104 cells, but not in the trans-complementing MA-NSP5 cell line
416 (Fig. 1C). Together, these data confirm that NSP5 is essential for RV replication.
417
418 **rRVs with impaired NSP5 phosphorylation**
419 To address the role of NSP5 hyperphosphorylation, we then generated a number
420 of rRVs harbouring NSP5 mutations previously known to impact NSP5
421 phosphorylation. We first generated an rRV carrying an S67A mutation (rRV-
422 NSP5/S67A) (Fig. S2 and Fig. 2A-B). This rRV strain appeared to be genetically
423 stable after a number of passages in the MA-NSP5 cell line (Fig. 2A-B). Its
424 replication in wild type MA104 cells was strongly impaired, resulting in
425 approximately a 100-fold reduction of the infectious progeny virus titre at different
426 time points post-infection (Fig. 2C). Despite the overall reduction of replication
427 fitness, the rRV-NSP5/S67A mutant virus was stable after at least 10 passages
428 in the wild-type MA104 cells. Consistent with our previous results, the NSP5-
429 S67A mutant was not hyper-phosphorylated in all cell lines tested, including
430 MA104, U2OS and Caco-2 cells (Fig. 2D), further confirming the role of Ser67 in
431 the initiation of NSP5 phosphorylation cascade [24]. While the wt rRV yielded

432 multiple hyper-phosphorylated NSP5 isoforms, the NSP5/S67A mutant mostly
433 produced a single non-phosphorylated NSP5 form with an apparent mass of 26
434 kDa that could be detected in the virus-infected cell extracts at 5 or 10 hpi (Fig.
435 2E). Enzymatic de-phosphorylation with λ-Ppase and alkaline Calf Intestinal
436 Ppase (CIP) further confirmed the observed lack of NSP5 phosphorylation (Fig.
437 2F). Because of the differences in the molecular weight markers used, the NSP5
438 band with the fastest PAGE mobility has been traditionally described as 26 kDa,
439 and the most abundant one as 28 kDa. Since this nomenclature has been used
440 in many publications, we have preferred to maintain it, despite current PAGE
441 migrations do not correspond to the markers presently used.
442 We then generated two additional rRVs harbouring truncated versions of NSP5,
443 one lacking the 18 AA long C-terminal tail (rRV-NSP5/ΔT), and the second one
444 with a 5 AA deletion (176-YKKKY-180) just upstream of the tail region (rRV-
445 NSP5/Δ176-180) (Fig. S2 and S3A-B). Despite the presence of Ser67, and the
446 lack of Thr and Ser residues within the deletions, both mutants did not show a
447 classical hyperphosphorylation pattern (Fig. 3A) and failed to replicate, confirmed
448 by the absence of *de novo* synthesis of genomic dsRNA (Fig. 3B).
449 We also investigated viroplasm formation in cells infected with these rRV
450 mutants. At early infection (5 hpi), the rRV-NSP5/S67A mutant produced
451 structures resembling viroplasms that appeared smaller and more
452 heterogeneous in shape compared to the regular spherical shaped ones
453 produced during the wt rRV infection (Fig 5A upper panel). Remarkably, during
454 late infection (10-12 hpi), the rRV-NSP5/S67A mutant produced multiple NSP5-
455 containing aberrant structures, as well as fibre-like structures that became more
456 apparent during late infection (12 hpi) (Fig. 4A lower panel).
457 Interestingly, the aberrant and fibre-like structures produced by rRV-NSP5/S67A
458 were morphologically similar to those observed during wt RV infection of MA104
459 cells silenced for cellular kinase CK1α, previously shown to be required for NSP5
460 phosphorylation [25]. NSP2-mCherry and NSP5-EGFP fusion proteins were also
461 recruited to both types of these structures (Fig. 4C-D), suggesting that the
462 observed lack of phosphorylation does affect NSP2/NSP5 interactions.

463 Furthermore, the non-phosphorylated NSP5 form co-localised with viroplasmic
464 proteins NSP2, VP6 and VP2 (Fig. 4B) that also localised to aberrant and fibre-
465 like structures, suggesting that they could also represent sites of virus replication.
466 In contrast, no viroplasms containing NSP5, NSP2 or VP2 were observed when
467 MA104 cells were infected with the rRV-NSP5/ΔT and rRV-NSP5/Δ176-180
468 deletion mutants. Interestingly, these mutants yielded only few fibre-like
469 structures containing VP6 protein (Fig. 4D-E). Similar VP6-fibres are normally
470 formed when VP6 is over-expressed in cells in the absence of other viral proteins
471 [35,36].
472 Taken together, these results confirm the essential role of NSP5 hyper-
473 phosphorylation for controlling the assembly of regular-shaped viroplasms,
474 highlighting the key role of the C-terminal tail in the formation of RV viral
475 factories.
476
477 **RNA accumulation in aberrant viroplasms**
478 Having examined the viral protein composition of the aberrant viroplasms formed
479 during infection with rRVs exhibiting impaired NSP5 phosphorylation, we then
480 assessed their RNA content. Viral RNA transcripts were labelled by incorporation
481 of 5-ethynyl uridine (5-EU) in actinomycin D-treated RV-infected cells, and total
482 viral ssRNA was visualized by reacting with Alexa-488-azide, as described in
483 Materials and Methods. As expected, most viral transcripts localised in
484 viroplasms of wt rRV-infected cells (Fig. 5A), consistent with the roles of
485 viroplasms in supporting the viral replication and assembly. In contrast, no viral
486 RNA transcripts could be detected in both wt MA104 or MA-NSP2-mCherry cells
487 infected with the rRV-NSP5/S67A mutant (Fig. 5A). RNA accumulation in
488 viroplasms was restored to almost identical levels as the wt rRVs when the rRV-
489 NSP5/S67A mutant was used to infect the MA-NSP5 cell line that supplies NSP5
490 in *trans* (Fig. 5A).
491 Although we did not detect RNA in rRV NSP5/S67A-infected MA104 cells using
492 5-EU staining, this mutant could still replicate (Fig. 2C). We then explored
493 whether rRV-NSP5/S67A transcripts could accumulate in viroplasms, albeit with

494 much lower efficiency, i.e., beyond the sensitivity limit of 5-EU staining. We used
495 single molecule RNA fluorescence in situ hybridisation (smFISH) to identify the
496 sites of RV transcription. At 10 hpi, abundant gs6 transcripts could be detected in
497 MA-NSP5-EGFP cells infected with the wild-type virus (Fig. 5B). Conversely, the
498 rRV-NSP5/S67A-infected cells had sparse EGFP-tagged viroplasms, also
499 containing gs6 RNA (Fig. 5B). Interestingly, the less frequently occurring rod-like
500 aberrant viroplasms also sustained gs6 RNA accumulation, further suggesting
501 that these structures could represent replication-functional organelles.
502 In contrast, smFISH performed on cells infected with the rRV-NSP5/ΔT showed
503 diffuse distribution of gs6 RNA that did not localise to any structures resembling
504 viroplasms (Fig. 5B), also failing to support the virus genome replication (Fig.
505 3B).
506 We then examined the ultrastructures of viroplasms with altered morphologies in
507 the RV mutant rRV-NSP5/S67A using electron microscopy. Upon infection with
508 rRV-wt (Fig. 6A, left panel), multiple membrane-less electron dense inclusions
509 encircled by the well-defined endoplasmatic reticulum (ER) filled with triple-
510 layered particles were present in cells. At late infection points (10 hpi), filled with
511 triple-layered particles (TLPs) ER appeared to adopt a more tubular morphology,
512 suggesting a successive step in the virus egress. In contrast, the rRV-
513 NSP5/S67A-infected cells contained only few immature viroplasms that lacked
514 the ER network filled with TLPs (Fig. 6A, right panel). Only few immature
515 particles containing transient lipid membranes could be identified in cells infected
516 with rRV-NSP5/S67A mutant (Fig. 6A, left panel). Furthermore, the observed
517 immature viroplasms also appeared to be less-electron dense, consistent with
518 their decreased capacity to accumulate viral RNAs.
519 Together, these data strongly support the role of NSP5 phosphorylation in
520 maintaining the viral RNA production and genome replication in viroplasms.
521
522 **The mechanism of NSP5 hyper-phosphorylation**
523 We have previously proposed a model of the hierarchical NSP5
524 hyperphosphorylation associated with the assembly of viroplasms that involves a

525 three-step mechanism: i) initial interaction of non-phosphorylated NSP5 with
526 NSP2 (or VP2); ii) phosphorylation of Ser67 by CK1α. This step does not take
527 place when NSP5 is expressed alone; iii) hyper-phosphorylation of NSP5
528 triggered by Ser67 phosphorylation that requires the 18 AA long C-terminal tail
529 [24].
530 Here, we have investigated the phosphorylation mechanism of NSP5 during RV
531 infection using a number of NSP5 phosphorylation-negative rRV strains and
532 MA104-derived stable transfectant cell lines (Fig. S2). We demonstrated that
533 despite the presence of Ser67, deletion mutant NSP5/ΔT was not phosphorylated
534 and failed to form viroplasms. We have previously shown that co-expression of
535 NSP5/ΔT was also unable to trigger the phosphorylation cascade of NSP5/S67A,
536 while other NSP5 mutants referred hereafter as activators of phosphorylation,
537 e.g., NSP5/Δ3 did [24]. Interestingly, upon co-infection with two rRVs NSP5/S67A
538 and NSP5/ΔT, both mutated NSP5 variants were not phosphorylated (Fig. 7A)
539 [8,19,24,26]. This result was supported further by infecting the MA104
540 transfectant cell line stably expressing NSP5-ΔT (MA-ΔT) with the rRV-
541 NSP5/S67A strain (Fig. S2 and Fig. 7B, lanes 3-4). The NSP5-Δ176-180 mutant
542 was also unable to induce phosphorylation of NSP5/S67A following the co-
543 infection with the two rRVs, despite both containing Ser67 and the C-terminal tail.
544 This result suggests that the 'activator' NSP5 needs to be also hyper-
545 phosphorylated (Fig. 7C).
546 In MA-ΔT cells infected with rRV-NSP5/S67A mutant strain aberrant viroplasms
547 were produced (Fig. 7E), similar to those seen in wt MA104 cells, which did not
548 support virus replication compared to the wt virus (Fig. 7F).
549 In contrast to NSP5/ΔT, the NSP5 deletion mutant lacking amino acids 80-130,
550 (NSP5/Δ3) becomes hyper-phosphorylated when expressed alone and can
551 function as an activator of the NSP5/S67A phosphorylation [19,24]. We therefore
552 asked whether an MA104 stable cell line expressing the deletion mutant
553 NSP5/Δ3 (MA-Δ3) and infected with the rRV-NSP5/S67A strain was able to
554 trigger hyperphosphorylation of NSP5/S67A and as a consequence, sustain

555 replication of the mutant rRV strain. As shown in Fig. 7B (lanes 5-6) NSP5/S67A
556 was hyper-phosphorylated in presence of NSP5/Δ3 mutant and confirmed by the
557 λPpase treatment (Fig. 7D), although it did not completely rescue the
558 phosphorylation pattern of NSP5 normally observed in rRV-wt infection.
559 Interestingly, regular round-shaped viroplasms, containing NSP5, NSP2 and VP2
560 with peripheral localisation of VP6, were recovered in these cells infected with
561 rRV-NSP5/S67A, and yet viral replication was nevertheless impaired (Fig. 7E-F).
562 Consistently, the electron microscopy images showed structures of aberrant
563 viroplasms similar to those obtained in MA104 wt cells (Fig. 6B, right panel).
564 The NSP5 phosphorylation negative mutants of the two other rRVs (NSP5/ΔT
565 and NSP5/Δ176-180), did not undergo hyper-phosphorylation in MA-ΔT or MA-Δ3
566 cell lines (Figs. 8A-B). In both cases, viroplasms formation and virus replication
567 were not rescued (Figs. 8C-D and 8E-F). Interestingly, apparently normal round-
568 shaped structures were observed in MA-Δ3 cells, which, however, recruited
569 significantly less VP6 (Fig. 8C-D). In addition, the previously observed VP6 spiky
570 structures were not detected in these cells (Figs. 8C-D). Similar results were
571 obtained with the rRV-NSP5/KO virus strain, which in MA-Δ3 cells did not
572 replicate and also showed spherical structures that contained NSP5 and NSP2,
573 but not VP6 (Fig. 9A-C).
574 Taken together, our data support a model of NSP5 hyper-phosphorylation, which
575 absolutely requires the presence of the C-terminal tail, and the AA residues 176-
576 180. Furthermore, NSP5 hyperphosphorylation requires Ser67 phosphorylation
577 to initiate the phosphorylation cascade, thus playing a key role in the assembly of
578 replication-competent viral factories.
579
580 **DISCUSSION**
581 Rotaviruses replicate within cytoplasmic viral factories, or viroplasms. Most RV
582 assembly intermediates, i.e., single layered particles (cores) and double-layered
583 particles (DLPs) are primarily concentrated in viroplasms. Following budding of
584 DLPs into the lumen of the endoplasmic reticulum, the immature particles acquire
585 a transient envelope, as well as the outer capsid proteins VP4 and VP7, resulting

586 in a mature triple-layered virion. Moreover, downregulation of expression of the
587 most abundant viroplasm-forming proteins NSP5 and NSP2 severely impacts on
588 the formation of viroplasms and production of virus progeny [13,15,25,34]. In light
589 of these observations, viroplasms have long been recognised as essential
590 compartments supporting the RV replication.
591 Of the two non-structural proteins involved in viroplasm assembly, NSP5 appears
592 to play a crucial role by potentially providing a scaffold that allows for recruitment
593 of additional viral proteins. Only when NSP5 is co-expressed with NSP2 and/or
594 VP2, these proteins assemble into the viroplasm-like structures (VLS), which are
595 also capable to recruit additional structural proteins including VP1, VP2 and VP6
596 [8,10]. Given these observations, we hypothesised that complete removal of
597 NSP5 would be lethal for RV replication. Using a modified reverse genetics
598 system for rotaviruses [29], here we provide the first direct evidence of the
599 essential role of NSP5 in viroplasm formation and viral replication. In order to
600 characterise replication-deficient NSP5-negative mutants, we have established a
601 trans-complementing system that provides NSP5 to the virus both transiently in
602 BHK-T7 cells, and stably in NSP5-producing MA104 cell line (MA-NSP5), thus
603 enabling facile isolation of rRVs lacking functional NSP5. Using this approach,
604 we have demonstrated that NSP5-deficient rRV was unable to form viroplasms
605 and replicate in the wt MA104 cells, while the viroplasm formation and viral
606 replication were efficiently rescued in the trans-complementing MA-NSP5 cell
607 line. Interestingly, the rRVs generated using this method also failed to
608 incorporate dsRNA originating from the NSP5-encoding mRNA lacking the 5' and
609 3' untranslated regions (UTRs), further suggesting the essential roles of UTRs for
610 genome packaging in RVs [37,38].
611 NSP5 hyper-phosphorylation has been previously implicated in the regulation of
612 NSP5 assembly into viroplasms. This phosphorylation, however, requires the
613 interaction of NSP5 with, either NSP2 or VP2, as NSP5 is not phosphorylated
614 when expressed alone [8,22,23]. Previous studies suggest that activation of
615 NSP5 hyper-phosphorylation may require a conformational change that leads to
616 its efficient hyper-phosphorylation via a positive feedback loop mechanism

617 [8,23,24]. Two regions comprising the N-terminal amino acids 1-33 (region 1) and
618 the central region amino acids 81-130 (region 3) have been reported to prevent
619 NSP5 phosphorylation in the absence of other viral proteins, while the 18 amino
620 acids long C-terminal tail was found to be essential for its phosphorylation
621 [8,23,24].
622 Here, we have shown that all three rRV mutants S67A, ΔT and Δ176-180
623 expressing the phosphorylation-negative NSP5 variants were unable to form
624 round-shaped viroplasms upon infection of MA104 cells. Interestingly, further
625 analysis of these mutants reveals some key differences between each NSP5
626 variant. While rRV-NSP5/S67A strain formed aberrant structures resembling
627 viroplasms that poorly support RV replication, this variant was still capable of
628 producing the infectious progeny, in contrast to the two other rRV mutant strains.
629 Interestingly, the phenotype observed with the NSP5 mutant S67A was
630 essentially the same as the one previously reported with the wt virus infecting
631 MA104 cells silenced for expression of CK1α, which is involved in
632 phosphorylating Ser67 and initiating the hyper-phosphorylation cascade [24,25].
633 It has recently been shown that CK1α is also involved in phosphorylating NSP2,
634 controlling the formation of rotavirus viral factories [39]. Our data obtained with
635 the rRV-NSP5/S67A mutant strongly suggest that the lack of NSP5 hyper-
636 phosphorylation determines both the morphogenesis of viroplasms and their
637 capacity to support RV genome replication. We cannot rule out the role of NSP2
638 phosphorylation in assembly of viroplasms since NSP2 is also likely to be
639 phosphorylated by CK1α upon infection of the rRV-NSP5/S67A strain. Despite
640 the formation of abnormal viroplasms and fibre-like structures, the amount of
641 RNA produced within those structures in rRV-NSP5/S67A-infected MA104 cells
642 was practically below the detection limit of the 5-EU labelling, while the RNA
643 replication was fully rescued in the trans-complementing MA-NSP5 cell line (Fig.
644 5). Interestingly, we were able to detect viral RNA in some of these aberrant
645 structures using RNA FISH with single molecule sensitivity. This result is
646 consistent with the finding that the rRV-NSP5/S67A strain did replicate, albeit at
647 much lower levels than the rRV-wt. Thus, these structures are likely to sustain

648 virus replication with decreased efficiency, which was further confirmed by the
649 electron microscopy analysis of MA104 cells infected with the rRV-NSP5/S67A
650 strain.
651 The essential role of NSP5 hyper-phosphorylation was further supported by the
652 results obtained with the two phosphorylation-negative mutant strains NSP5/ΔT
653 and NSP5/Δ176-180 that possess Ser67 and yet failed to form viroplasms.
654 Surprisingly, the Δ176-180 mutant, containing the C-terminal tail has also failed
655 to form viroplasms, despite the absence of Ser or Thr within the chosen 176-180
656 region. Both phosphorylation-negative mutants tested did not replicate in MA104
657 cells and we could not detect any structures containing viral RNA.
658 Using the NSP5 mutant strains described above and the established stable
659 transfectant MA104 cells we were able to investigate the molecular mechanism
660 that leads to NSP5 hyperphosphorylation. We showed that the NSP5/S67A
661 mutant from the rRV was indeed hyperphosphorylated, albeit not completely,
662 when infecting MA-Δ3 cells, restoring round-shaped viroplasms with a complete
663 absence of the fibre-like structures observed in MA104 cells. This finding strongly
664 suggests that impairment of NSP5 phosphorylation is the direct cause of the
665 formation of both aberrant and fibre-like structures. Despite the fact that
666 viroplasms appeared morphologically normal in MA-Δ3 cells, recruitment of VP6
667 at the periphery of viroplasms was only observed with the hyperphosphorylated
668 NSP5/S67A mutant, in contrast to the other NSP5 phosphorylation negative
669 mutants. One possibility is that recruitment of VP6 to round-shaped viroplasms
670 requires a full-length hyperphosphorylated NSP5, as well as phosphorylation of
671 multiple serine residues likely by CK2 [17,26]. Moreover, the round-shaped
672 structures found in MA-Δ3 cells infected with rRV-NSP5/KO failed to recruit VP6.
673 The observed failure to rescue the replication of the rRV-NSP5/S67A strain to the
674 wt levels in MA-Δ3 cells could be the consequence of the incomplete recovery of
675 the complex pattern of phosphorylated isoforms of wt NSP5. This suggests that
676 some intermediate isoforms might be important for the formation of fully
677 functional replication-competent viroplasms.

678 We propose a model of the complex hierarchical mechanism of NSP5 hyper-
679 phosphorylation during RV infection (Fig. 10). It involves (a) interaction of NSP5
680 with either NSP2 or VP2, required to (b) make Ser67 available for CK1α
681 phosphorylation. This initial step is then sequentially completed (c) by CK2-
682 mediated phosphorylation of other serines to generate the NSP5 'activator',
683 during a step dependent (d) on the interaction of the Ser67-phosphorylated
684 molecules with the non-phosphorylated partners in the NSP5 oligomeric
685 complexes. Alternatively (c'), oligomers could be formed before the activation
686 step. NSP5 interactions mediated by the carboxy-terminal tails T result in (e)
687 substrate activation and a fully hyperphosphorylated NSP5. This process leads to
688 (f) the assembly of viroplasms scaffolds containing NSP2, and (g) recruitment of
689 VP6, as well as the other viroplasmic proteins, VP1, VP2, VP3 to assemble
690 replication-competent viroplasms.
691 The hierarchical phosphorylation of proteins appears to be a common
692 mechanism regulating many cellular processes. In mammalian cells, hierarchical
693 phosphorylation has been described for β-catenin, in which Ser 45
694 phosphorylated by CK1α primes it for hyperphosphorylation by glycogen
695 synthase kinase-3 (GSK-3) [40,41], which triggers its ubiquitination and
696 proteasomal degradation [42]. A similar phosphorylation mechanism has recently
697 been described for a non-structural protein NS5A of the Hepatitis C Virus (HCV),
698 with the hyper-phosphorylation cascade primed by the initial phosphorylation of
699 Serine 225 by CK1α, and the subsequent phosphorylation of neighbouring
700 residues involving other kinases [43,44]. Moreover, the NS5A phosphorylation
701 was shown to play a key role in controlling the establishment of replication
702 complexes during HCV infection [45]. Similarly, a number of other non-structural
703 viral proteins have been shown to undergo multiple phosphorylation events
704 during virus infection, suggesting that this complex post-translational
705 modifications play a pivotal role in orchestrating the assembly of replication-
706 competent viral factories [46–48].
707
708

ACKNOWLEDGEMENTS

We thank John T. Patton, Asha Ann Philipp and Jin Dai (Indiana University, Bloomington, USA), Yuta Kanai and Takeshi Kobayashi (Fujita Health University, Aichi) and Albie Van Dijik (North-West University, South Africa) for helpful discussions on the establishment of the reverse genetics system. We are grateful to Naoto Ito for providing BHK-T7 cells.

740 **FIGURE LEGENDS**

741

742 **Fig. 1. Characterisation of rRV-NSP5/KO.** A) Western blot of MA104 cells
743 extracts infected with rRV-wt and rRV-NSP5/KO strains (MOI 1 FFU/cell). B)
744 Confocal immunofluorescence microscopy of MA104, MA-NSP2-mCherry and
745 MA-NSP5-EGFP cells infected with rRV-wt or rRV-NSP5/KO (MOI 1 FFU/cell),
746 using antibodies for NSP5, NSP2, VP2 and VP6, as indicated. Scale bar, 15 μm.
747 C) Electrophoretic migration pattern of dsRNAs extracted from rRV-NSP5/KO
748 strain grown in MA-NSP5 or MA104 cells. Genome segments 1-11 are indicated
749 to the left.

750

751 **Fig 2. Characterisation of rRV-NSP5/S67A.** A) Schematic representation of
752 rRV-NSP5/S67A gs11 and sequence of NSP5 wt and S67A mutant (highlighted).
753 B) Electrophoretic pattern of dsRNA genome segments of rRV-wt and rRV-
754 NSP5/S67A strains grown in MA-NSP5 cells. C) Replication kinetics of rRV-wt
755 and rRV-NSP5/S67A in MA104 cells. Data are expressed as the means +/-
756 standard deviations (n=3); ***, $p < 0.001$ (Student's t test). D) Western blot of
757 extracts of U2OS, Caco-2 and MA104 cells infected with rRV-wt or rRV-
758 NSP5/S67A strains. E) Western blot of NSP5 phosphorylation pattern in MA104
759 cells infected with rRV-wt or rRV-NSP5/S67A (MOI 1 FFU/cell) at 5 and 10 hpi. F)
760 Western blot of λ-Ppase and alkaline Ppase treatment of lysates of MA104 cells
761 infected with rRV-wt or rRV-NSP5/S67A. The NSP5 proteins are shown.

762

763 **Fig 3. Characterisation of rRV-NSP5/ΔT and rRV-NSP5/Δ176-180.** A) Western
764 blot of NSP5 and NSP5 mutants from MA104 cells infected with rRV-wt, rRV-
765 NSP5/ΔT or rRV- NSP5/Δ176-180 at 5 hpi. B) Electrophoretic dsRNA migration
766 pattern of rRV-NSP5/ΔT and rRV-NSP5/Δ176-180 grown in MA-NSP5 and
767 MA104 cells.

768

769 **Fig 4. Viroplasms morphology in MA104 cells infected with rRV-NSP5 wt**
770 **and mutants.** Representative confocal immunofluorescence micrographs of

771 MA104 cells infected with rRV-wt and rRV-NSP5/S67A (MOI 15 FFU/cell) at 5 hpi
772 (upper panels) or 10 hpi (lower panels). Cells were stained with anti-NSP5 and
773 DAPI. B) Confocal immunofluorescence micrographs of rRV-wt and rRV-
774 NSP5/S67A infected MA104 cells (MOI 15 FFU/cell) and stained at 10 hpi with
775 the indicated antibodies. C) Confocal immunofluorescence micrographs of MA-
776 NSP5-EGFP and MA-NSP2-mCherry cells infected with rRV-NSP5/S67A (MOI
777 15 FFU/cell). D), E), Confocal immunofluorescence of MA104 cells infected with
778 rRV-NSP5/Δ176-180 (D) or rRV-NSP5/ΔT (E) and stained with the indicated
779 antibodies and DAPI. Scale bar, 15 μm.
780
781 **Fig 5. Viral RNA detection in rRV NSP5/S67A infected cells**. A)
782 Representative confocal immunofluorescence micrographs of MA104 (upper
783 panel), MA-NSP5 (middle panel) and MA-NSP2-mCherry cells (lower panel)
784 infected with rRV-wt or rRV-NSP5/S67A strains and stained with anti-NSP5 (red,
785 in MA104 and MA-NSP5 cells) and EU (green). B) Single molecule RNA
786 Fluorescence In Situ Hybridisation (smFISH) on MA-NSP5-EGFP cells infected
787 with rRV-wt, rRV-NSP5/S67A or rRV-NSP5/ΔT strains. Viroplasms detected with
788 NSP5-EGFP (green) and viral RNA (probe specific for gs6 was Cy3-conjugated,
789 red). Co-localization of viroplasms and RNA is indicated by white arrows. Scale
790 bar, 15 μm.
791
792 **Fig 6. Electron microscopy of cells infected with rRV-NSP5/S67A.** High–
793 definition electron micrographs of MA104 (A) and MA-Δ3 (B) cells infected with
794 rRV-wt (left panel) and rRV-NSP5/S67A (right panel) (MOI, 75 FFU/cell). At 10
795 hpi, cells were fixed with glutaraldehyde and processed for transmission electron
796 microscopy. V, viroplasm; m, mitochondria; mt, microtubule-bundles; Nu, nucleus.
797 The white open box indicates the immediate right magnified image. White arrows
798 indicate the endoplasmic reticulum surrounding viroplasms; black arrowheads
799 indicate viral particles with an envelope. Scale bar, 500 nm.
800

801 **Fig 7. Phosphorylation of NSP5/S67A**. A) Western blot of extracts of MA104
802 cells infected with rRV-NSP5/S67A or co-infected with rRV-NSP5/S67A and rRV-
803 NSP5/ΔT. Blue arrowhead indicates NSP5/S67A. The faster migrating band
804 corresponds to NSP5-ΔT. B) Western blot of MA104, MA-ΔT and MA-Δ3 cells
805 infected with rRV-NSP5/S67A. Blue arrowhead indicates NSP5/S67A. C)
806 Western blot of extracts of MA104 cells co-infected with rRV-NSP5/S67A and
807 rRV-NSP5/Δ176-180. Blue arrowhead indicates NSP5/S67A. D) λ-Ppase
808 treatment of extracts of MA-Δ3 cells infected with the rRV-NSP5/S67A strain.
809 Filled and open arrowheads indicate de-phosphorylated NSP5-S67A and NSP5-
810 Δ3, respectively. E) Representative confocal immunofluorescence micrographs of
811 MA104, MA-ΔT and MA-Δ3 cells infected with rRV-NSP5/S67A. Cells were
812 stained with the indicated antibodies. Scale bar, 15 μm. F) Yield of infectious
813 virus of rRV-NSP5/S67A grown in MA-NSP5, MA104, MA-ΔT and MA-Δ3 cells at
814 24 hpi.*, $p < 0.05$; **, $p < 0.01$.
815
816 **Fig 8. Phosphorylation of NSP5/-ΔT and NSP5/Δ176-180 and viroplasm**
817 **formation**. Western blots (A, B) and confocal immunofluorescence micrographs
818 (C, D) of MA104, MA-ΔT and MA-Δ3 cells infected with rRV-NSP5/ΔT (A, C) or
819 with rRV-NSP5/Δ176-180 (B, D). Blue arrowhead indicates NSP5/ΔT and
820 NSP5/Δ176-180, respectively. Open arrowheads indicate NSP5-Δ3 and NSP5-
821 ΔT. Cells were stained with the indicated antibodies and DAPI. Scale bar, 15 μm.
822 E) Single step growth of rRV-NSP5/ΔT (left) and rRV-NSP5/Δ176-180 (right) in
823 MA-NSP5, MA104, MA-ΔT and MA-Δ3 cells, as indicated. The experiment was
824 terminated at 24 hpi. **, $p < 0.01$; #, Viral titer < 300 FFU/ml.
825
826 **Fig 9. rRV NSP5/KO in infected cells**. Western blot (A) and confocal
827 immunofluorescence (B) of MA104, MA-ΔT and MA-Δ3 cells infected with the
828 rRV-NSP5/KO strain. Cells were stained with the indicated antibodies and DAPI.
829 Scale bar, 15 μm. C) Single step growth of rRV-NSP5/KO in MA-NSP5, MA104,
830 MA-ΔT and MA-Δ3 cells, as indicated. The experiment was terminated at 24 hpi.
831 **, $p < 0.01$; #, Viral titer < 300 FFU/ml.

832

833 **Fig 10. Model of NSP5 hyperphosphorylation and assembly of replication-**
834 **competent viroplasms.** (***a***) Interaction of non-phosphorylated NSP5 with either
835 NSP2 or VP2 is required to (***b***) induce conformational changes that make S67
836 available for CK1α phosphorylation (P). This initial step of the cascade is then (***c***)
837 sequentially completed by phosphorylation by CK2 of other residues including
838 serines in domain 4, to generate the NSP5 activator or, (***c'***) a step of interaction
839 with non-phosphorylated molecule precedes the involvement of CK2. (***d***) NSP5
840 interactions to form dimers/multimers are mediated by the carboxy-terminal tails
841 (T). (***e***) The primed (S67-phosphorylated) activator molecules result in substrate
842 activation and fully hyper-phosphorylated NSP5. (***f***) Assembly of viroplasms
843 scaffolds containing NSP2 serve to (***g***) recruit the other viroplasmic components,
844 VP1, VP2, VP3 and VP6 to assemble replication-competent viroplasms. P;
845 phosphorylated amino acid. *This image was created using BioRender.com.

846

847 **Fig S1.** Schematic representation of the modified reverse genetics protocol used
848 to rescue rRV with mutations in genome segment 11. gs; genome segment
849 *Created using BioRender.com.

850

851 **Fig S2.** Schematic representation of the different NSP5 or NSP2 mutants or
852 fusion proteins used to generate rRV or stable MA104 transfectant cell lines (or
853 both) and used in this study. *Created using BioRender.com

854 **Fig S3.** A) Schematic representation of mutations in gs11 of the corresponding
855 rRV strains. Sequences mutated or deleted in NSP5 are indicated. B), Profiles of
856 viral dsRNAs of the different rRV strains generated. gs11, indicated in red with *.

857

858

859

860 **REFERENCES**

861 1. Tate JE, Burton AH, Boschi-Pinto C, Parashar UD, World Health
862 Organization–Coordinated Global Rotavirus Surveillance Network. Global,
863 Regional, and National Estimates of Rotavirus Mortality in Children <5
864 Years of Age, 2000–2013. Clin Infect Dis. 2016;62: S96–S105.
865 doi:10.1093/cid/civ1013

866 2. Parashar UD, Hummelman EG, Bresee JS, Miller MA, Glass RI. Global
867 illness and deaths caused by rotavirus disease in children. Emerg Infect
868 Dis.; 2003;9: 565–572.

869 3. Patton JT, Silvestri LS, Tortorici MA, Vasquez-Del Carpio R, Taraporewala
870 ZF. Rotavirus genome replication and morphogenesis: role of the
871 viroplasm. Curr Top Microbiol Immunol. 2006;309: 169–87.

872 4. Desselberger U. Rotaviruses. Virus Res; 2014;190: 75–96.
873 doi:10.1016/j.virusres.2014.06.016

874 5. Estes MK, Greenberg HB. Rotaviruses. In: Health WK, Lippincott Williams
875 Wilkins, editors. Fields Virology. 6th ed. Philadelpia, PA; 2013. pp. 1347–
876 1401.

877 6. Clapp LL, Patton JT. Rotavirus morphogenesis: domains in the major inner
878 capsid protein essential for binding to single-shelled particles and for
879 trimerization. Virology; 1991;180: 697–708.

880 7. Eichwald C, Rodriguez JF, Burrone OR. Characterization of rotavirus
881 NSP2/NSP5 interactions and the dynamics of viroplasm formation. J Gen
882 Virol. 2004;85: 625–634. doi:10.1099/vir.0.19611-0

883 8. Fabbretti E, Afrikanova I, Vascotto F, Burrone OR. Two non-structural
884 rotavirus proteins, NSP2 and NSP5, form viroplasm-like structures in vivo.
885 J Gen Virol. 1999;80: 333–339. doi:10.1099/0022-1317-80-2-333

886 9. Poncet D, Lindenbaum P, L'Haridon R, Cohen J. In vivo and in vitro
887 phosphorylation of rotavirus NSP5 correlates with its localization in
888 viroplasms. J Virol. 1997;71: 34–41.

889 10. Arnoldi F, Campagna M, Eichwald C, Desselberger U, Burrone OR.
890 Interaction of Rotavirus Polymerase VP1 with Nonstructural Protein NSP5
891 Is Stronger than That with NSP2. J Virol. 2007;81: 2128–2137.
892 doi:10.1128/JVI.01494-06

893 11. Gallegos CO, Patton JT. Characterization of rotavirus replication
894 intermediates: a model for the assembly of single-shelled particles.
895 Virology. 1989;172: 616–27.

896 12. Campagna M, Eichwald C, Vascotto F, Burrone OR. RNA interference of
897 rotavirus segment 11 mRNA reveals the essential role of NSP5 in the virus
898 replicative cycle. J Gen Virol; 2005;86: 1481–1487.
899 doi:10.1099/vir.0.80598-0

900 13. Lopez T, Rojas M, Ayala-Breton C, Lopez S, Arias CF. Reduced
901 expression of the rotavirus NSP5 gene has a pleiotropic effect on virus
902 replication. J Gen Virol. 2005;6: 1609–1617.

903 14. Silvestri LS, Taraporewala ZF, Patton JT. Rotavirus replication: plus-sense
904 templates for double-stranded RNA synthesis are made in viroplasms. J
905 Virol. American Society for Microbiology; 2004;78: 7763–74.
906 doi:10.1128/JVI.78.14.7763-7774.2004

907 15. Vascotto F, Visintin M, Cattaneo A, Burrone OR. Design and selection of
908 an intrabody library produced de-novo for the non-structural protein NSP5
909 of rotavirus. J Immunol Methods; 2005;301: 31–40.

910 16. Gonzalez SA, Burrone OR. Rotavirus NS26 is modified by addition of
911 single O-linked residues of N-acetylglucosamine. Virology. 1991;182: 8–16.

912 17. Sotelo PH, Schumann M, Krause E, Chnaiderman J. Analysis of rotavirus

913 non-structural protein NSP5 by mass spectrometry reveals a complex
914 phosphorylation pattern. Virus Res. 2010;149: 104–108.

915 18. Campagna M, Marcos-Villar L, Arnoldi F, de la Cruz-Herrera CF, Gallego
916 P, Gonzalez-Santamaria J, et al. Rotavirus Viroplasm Proteins Interact with
917 the Cellular SUMOylation System: Implications for Viroplasm-Like
918 Structure Formation. J Virol. 2013;87: 807–817. doi:10.1128/JVI.01578-12

919 19. Afrikanova I, Miozzo MC, Giambiagi S, Burrone O. Phosphorylation
920 generates different forms of rotavirus NSP5. J Gen Virol. 1996;9: 2059–
921 2065.

922 20. Blackhall J, Fuentes A, Hansen K, Magnusson G. Serine protein kinase
923 activity associated with rotavirus phosphoprotein NSP5. J Virol. 1997;71:
924 138–144.

925 21. Eichwald C, De Lorenzo G, Schraner EM, Papa G, Bollati M, Swuec P, et
926 al. Identification of a Small Molecule That Compromises the Structural
927 Integrity of Viroplasms and Rotavirus Double-Layered Particles. J Virol.
928 American Society for Microbiology (ASM); 2018;92. doi:10.1128/JVI.01943-
929 17

930 22. Contin R, Arnoldi F, Campagna M, Burrone OR. Rotavirus NSP5
931 orchestrates recruitment of viroplasmic proteins. J Gen Virol. 2010;7:
932 1782–1793.

933 23. Afrikanova I, Fabbretti E, Miozzo MC, Burrone OR. Rotavirus NSP5
934 phosphorylation is up-regulated by interaction with NSP2. J Gen Virol.
935 1998;79: 2679–2686. doi:10.1099/0022-1317-79-11-2679

936 24. Eichwald C, Jacob G, Muszynski B, Allende JE, Burrone OR. Uncoupling
937 substrate and activation functions of rotavirus NSP5: phosphorylation of
938 Ser-67 by casein kinase 1 is essential for hyperphosphorylation. Proc Natl
939 Acad Sci U S A. 2004;101: 16304–16309.

940 25. Campagna M, Budini M, Arnoldi F, Desselberger U, Allende JE, Burrone
941 OR. Impaired hyperphosphorylation of rotavirus NSP5 in cells depleted of
942 casein kinase 1alpha is associated with the formation of viroplasms with
943 altered morphology and a moderate decrease in virus replication. J Gen
944 Virol. 2007;10: 2800–2810.

945 26. Eichwald C, Vascotto F, Fabbretti E, Burrone OR. Rotavirus NSP5:
946 mapping phosphorylation sites and kinase activation and viroplasm
947 localization domains. J Virol. 2002;76: 3461–3470.

948 27. Martin D, Ouldali M, Menetrey J, Poncet D. Structural organisation of the
949 rotavirus nonstructural protein NSP5. J Mol Biol. 2011;413: 209–221.

950 28. Kanai Y, Komoto S, Kawagishi T, Nouda R, Nagasawa N, Onishi M, et al.
951 Entirely plasmid-based reverse genetics system for rotaviruses. Proc Natl
952 Acad Sci U S A. National Academy of Sciences; 2017;114: 2349–2354.
953 doi:10.1073/pnas.1618424114

954 29. Komoto S, Fukuda S, Ide T, Ito N, Sugiyama M, Yoshikawa T, et al.
955 Generation of Recombinant Rotaviruses Expressing Fluorescent Proteins
956 by Using an Optimized Reverse Genetics System. J Virol. 2018;92:
957 e00588-18. doi:10.1128/JVI.00588-18

958 30. Pertel T, Hausmann S, Morger D, Züger S, Guerra J, Lascano J, et al.
959 TRIM5 is an innate immune sensor for the retrovirus capsid lattice. Nature.
960 2011;472: 361–365. doi:10.1038/nature09976

961 31. Dull T, Zufferey R, Kelly M, Mandel RJ, Nguyen M, Trono D, et al. A third-
962 generation lentivirus vector with a conditional packaging system. J Virol.
963 1998;72: 8463–71.

964 32. Yusa K, Zhou L, Li MA, Bradley A, Craig NL. A hyperactive piggyBac
965 transposase for mammalian applications. Proc Natl Acad Sci U S A.
966 National Academy of Sciences; 2011;108: 1531–6.

967 doi:10.1073/pnas.1008322108

968 33. Eichwald C, Arnoldi F, Laimbacher AS, Schraner EM, Fraefel C, Wild P, et
969 al. Rotavirus viroplasm fusion and perinuclear localization are dynamic
970 processes requiring stabilized microtubules. PLoS One. Public Library of
971 Science; 2012;7: e47947. doi:10.1371/journal.pone.0047947

972 34. Vascotto F, Campagna M, Visintin M, Cattaneo A, Burrone OR. Effects of
973 intrabodies specific for rotavirus NSP5 during the virus replicative cycle. J
974 Gen Virol.; 2004;85: 3285–3290.

975 35. Ito H, Minamoto N, Goto H, Rong LT, Sugiyama M, Kinjo T. Expression of
976 the major inner capsid protein, VP6, of avian rotavirus in mammalian cells.
977 Vet Microbiol. 1996;49: 257–65.

978 36. Tosser G, Labbé M, Brémont M, Cohen J. Expression of the major capsid
979 protein VP6 of group C rotavirus and synthesis of chimeric single-shelled
980 particles by using recombinant baculoviruses. J Virol. American Society for
981 Microbiology (ASM); 1992;66: 5825–31.

982 37. McDonald SM, Patton JT. Assortment and packaging of the segmented
983 rotavirus genome. Trends Microbiol. Elsevier Ltd; 2011;19: 136–144.
984 doi:10.1016/j.tim.2010.12.002

985 38. Borodavka A, Desselberger U, Patton JT. Genome packaging in multi-
986 segmented dsRNA viruses: distinct mechanisms with similar outcomes.
987 Curr Opin Virol. Elsevier; 2018;33: 106–112.
988 doi:10.1016/J.COVIRO.2018.08.001

989 39. Criglar JM, Anish R, Hu L, Crawford SE, Sankaran B, Prasad BVV, et al.
990 Phosphorylation cascade regulates the formation and maturation of
991 rotaviral replication factories. Proc Natl Acad Sci. 2018;115: E12015–
992 E12023. doi:10.1073/pnas.1717944115

993 40. Liu C, Li Y, Semenov M, Han C, Baeg GH, Tan Y, et al. Control of beta-

994 catenin phosphorylation/degradation by a dual-kinase mechanism. Cell.
995 2002;108: 837–47.

996 41. Amit S, Hatzubai A, Birman Y, Andersen JS, Ben-Shushan E, Mann M, et
997 al. Axin-mediated CKI phosphorylation of β-catenin at Ser 45: A molecular
998 switch for the Wnt pathway. Genes Dev. 2002; doi:10.1101/gad.230302

999 42. Verheyen EM, Gottardi CJ. Regulation of Wnt/β-catenin signaling by
1000 protein kinases. Developmental Dynamics. 2010. doi:10.1002/dvdy.22019

1001 43. Goonawardane N, Yin C, Harris M. A pivotal role of serine 225
1002 phosphorylation in the function of hepatitis C virus NS5A revealed with the
1003 application of a phosphopeptide antiserum and super-resolution
1004 microscopy. bioRxiv. 2018; doi:10.1101/387407

1005 44. Kim J, Lee D, Choe J. Hepatitis C virus NS5A protein is phosphorylated by
1006 casein kinase II. Biochem Biophys Res Commun; 1999;257: 777–781.

1007 45. Ross-Thriepland D, Mankouri J, Harris M. Serine Phosphorylation of the
1008 Hepatitis C Virus NS5A Protein Controls the Establishment of Replication
1009 Complexes. Diamond MS, editor. J Virol. 2015;89: 3123–3135.
1010 doi:10.1128/JVI.02995-14

1011 46. Keating JA, Bhattacharya D, Lim P-Y, Falk S, Weisblum B, Bernard KA, et
1012 al. West Nile virus methyltransferase domain interacts with protein kinase
1013 G. Virol J. BioMed Central; 2013;10: 242. doi:10.1186/1743-422X-10-242

1014 47. Spencer K-A, Dee M, Britton P, Hiscox JA. Role of phosphorylation
1015 clusters in the biology of the coronavirus infectious bronchitis virus
1016 nucleocapsid protein. Virology. 2008;370: 373–381.
1017 doi:10.1016/j.virol.2007.08.016

1018 48. Bhattacharya D, Hoover S, Falk SP, Weisblum B, Vestling M, Striker R.
1019 Phosphorylation of yellow fever virus NS5 alters methyltransferase activity.
1020 Virology. 2008;380: 276–284. doi:10.1016/j.virol.2008.07.013

1021

Figure S1

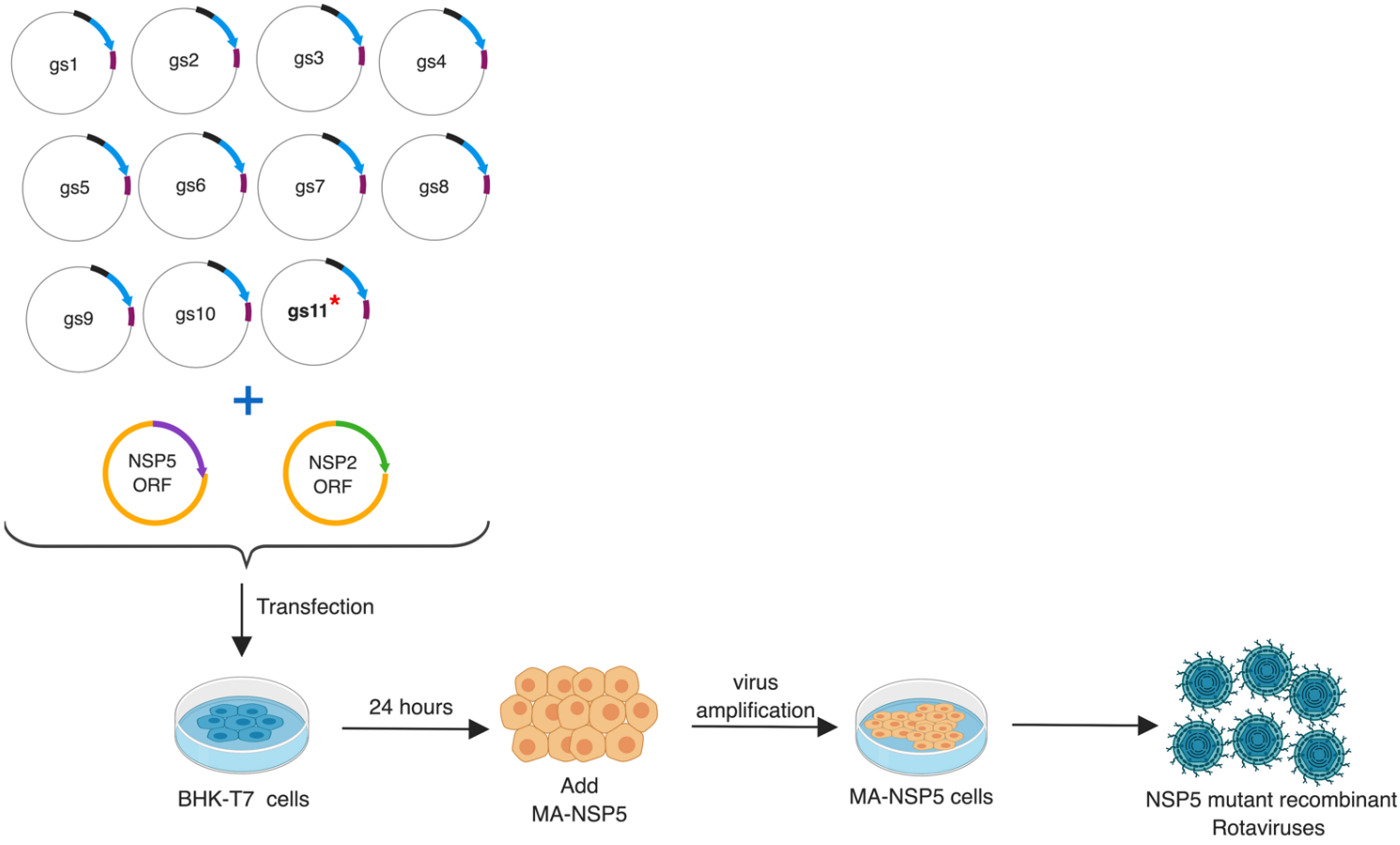
gs1
gs2
gs3
gs4
gs5
gs6
gs7
gs8
gs9
gs10
gs11*
+
NSP5 ORF
NSP2 ORF
Transfection
BHK-T7 cells
24 hours
Add MA-NSP5
virus amplification
MA-NSP5 cells
NSP5 mutant recombinant Rotaviruses

Figure S2

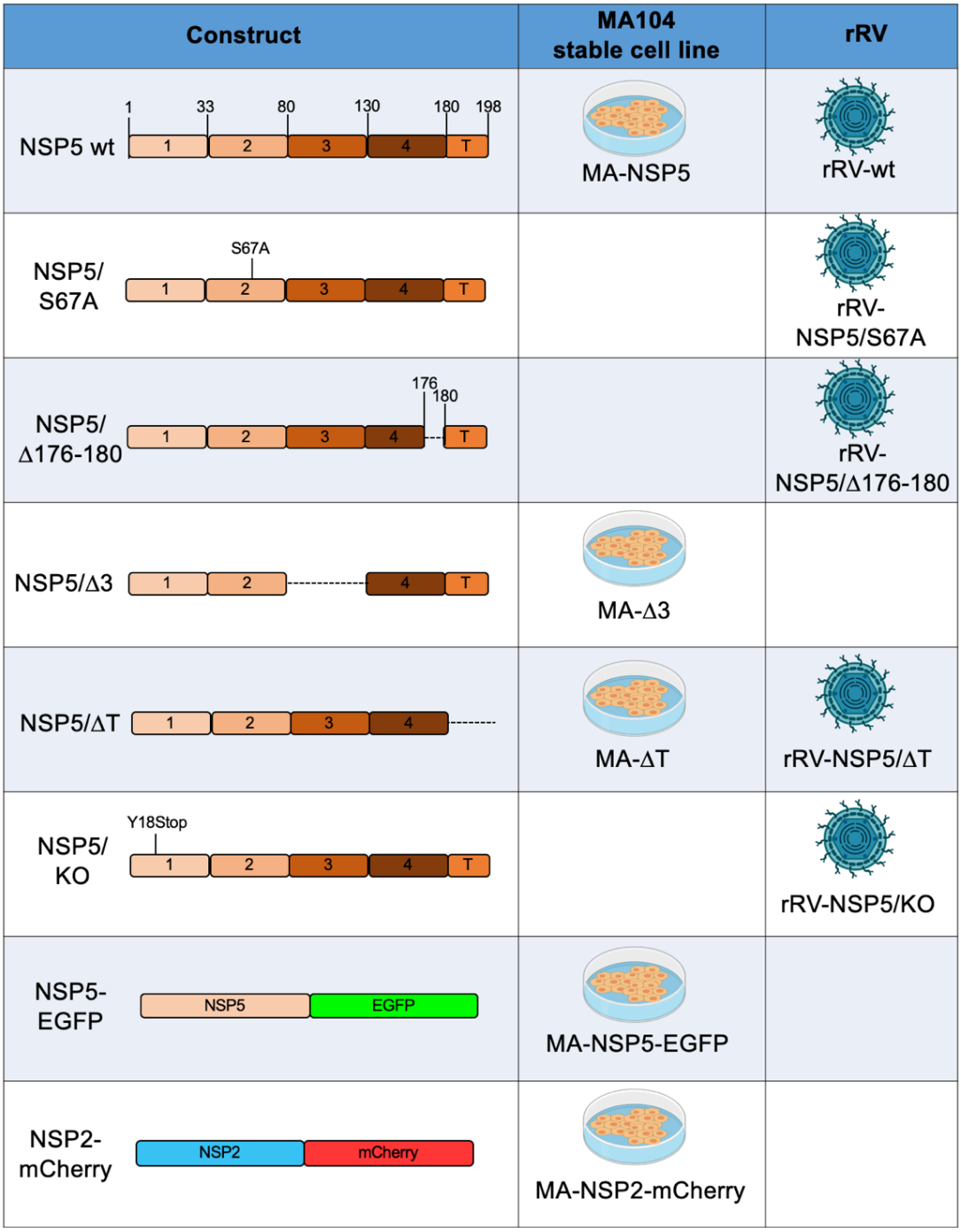
Construct
MA104 stable cell line
rRV
NSP5 wt
1
33
80
130
180
198
1
2
3
4
T
MA-NSP5
rRV-wt
NSP5/ S67A
S67A
rRV- NSP5/S67A
NSP5/ Δ176-180
176
180
rRV- NSP5/Δ176-180
NSP5/Δ3
MA-Δ3
NSP5/ΔT
MA-ΔT
rRV-NSP5/ΔT
NSP5/ KO
Y18Stop
rRV-NSP5/KO
NSP5- EGFP
NSP5
EGFP
MA-NSP5-EGFP
NSP2- mCherry
NSP2
mCherry
MA-NSP2-mCherry

Figure S3

A

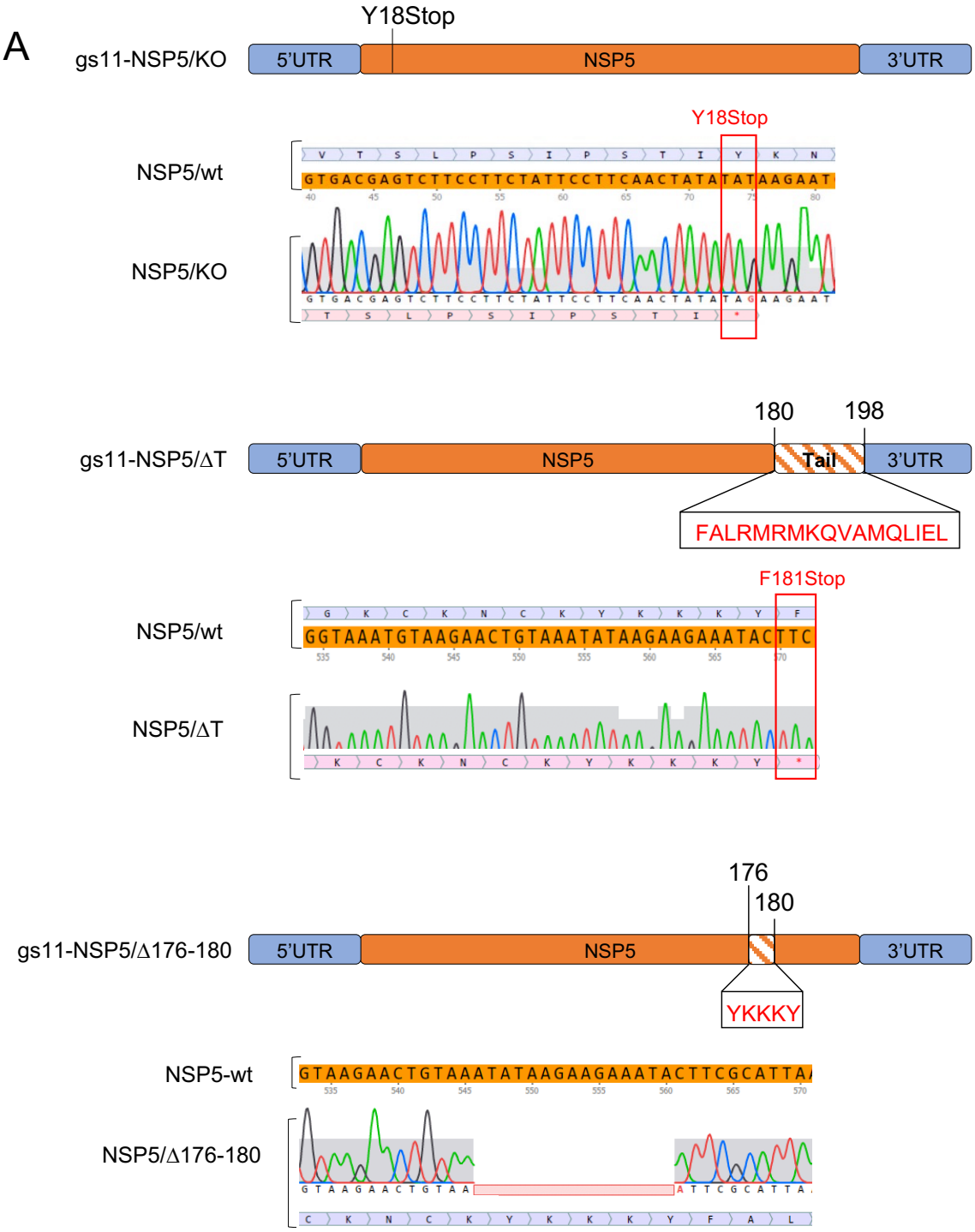
gs11-NSP5/KO
Y18Stop
5'UTR
NSP5
3'UTR
NSP5/wt
NSP5/KO
gs11-NSP5/ΔT
180
198
Tail
FALRMRMKQVAMQLIEL
F181Stop
NSP5/ΔT
gs11-NSP5/Δ176-180
176
180
YKKKY
NSP5-wt
NSP5/Δ176-180

B

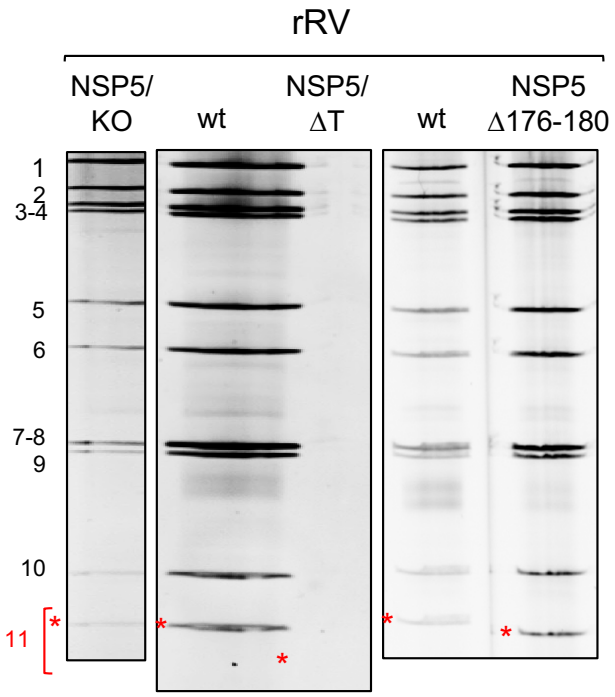
rRV
NSP5/ KO
wt
NSP5/ ΔT
wt
NSP5 Δ176-180
1
2
3-4
5
6
7-8
9
10
11

Figure 1

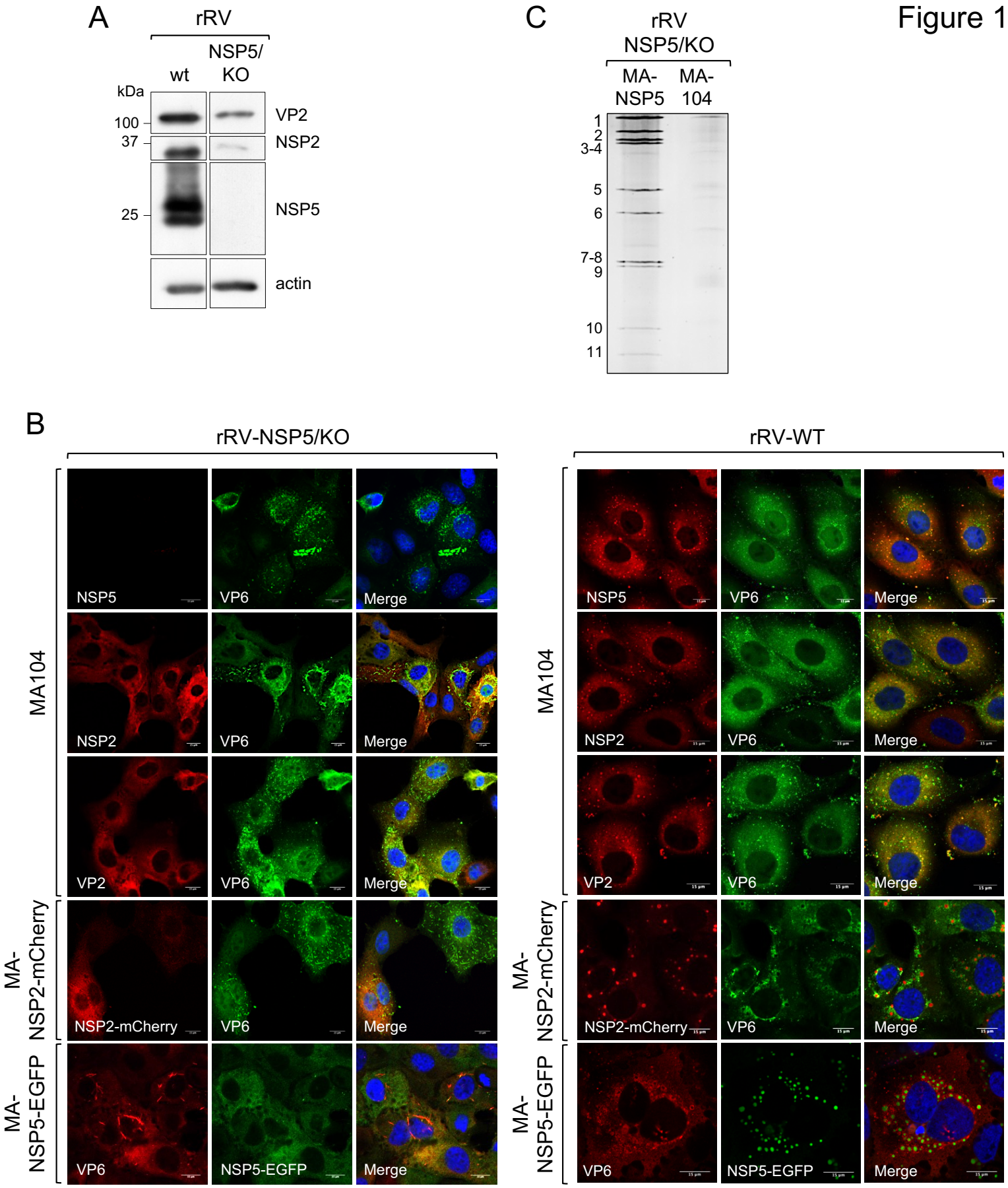
A
rRV
wt
NSP5/
KO
kDa
100
37
25
VP2
NSP2
NSP5
actin
C
rRV
NSP5/KO
MA-
NSP5
MA-
104
1
2
3-4
5
6
7-8
9
10
11
B
rRV-NSP5/KO
rRV-WT
MA104
MA-
NSP2-mCherry
MA-
NSP5-EGFP
NSP5
VP6
Merge
NSP2
VP2
NSP2-mCherry
NSP5-EGFP

Figure 2

A

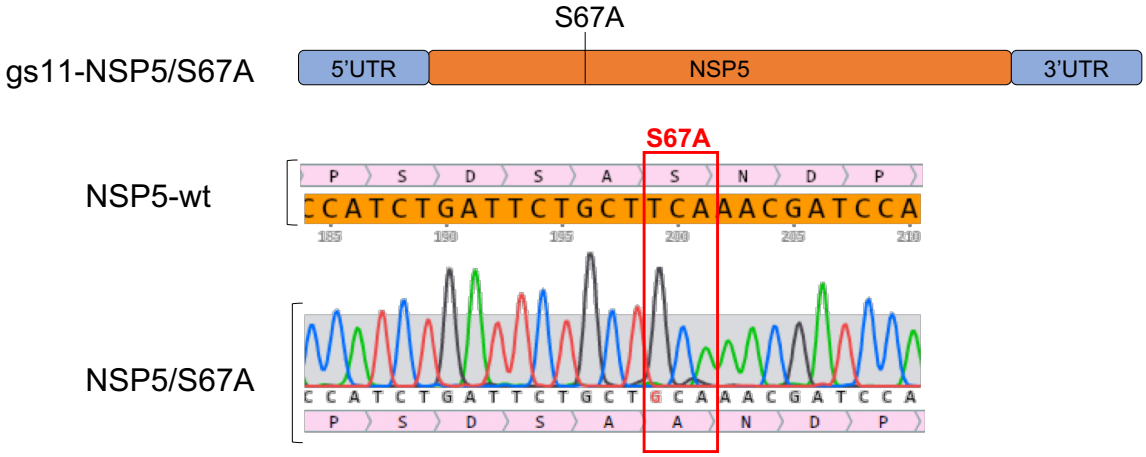

B

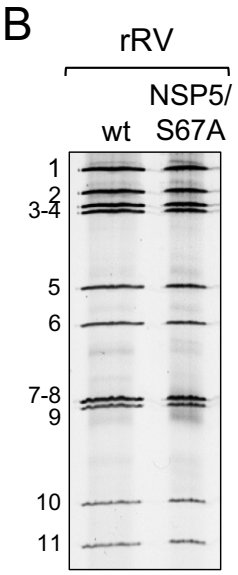

C

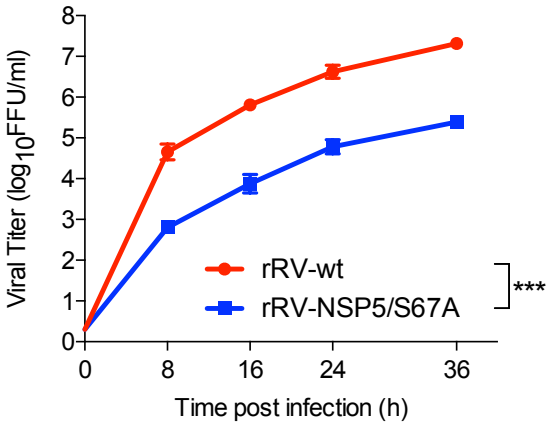

D

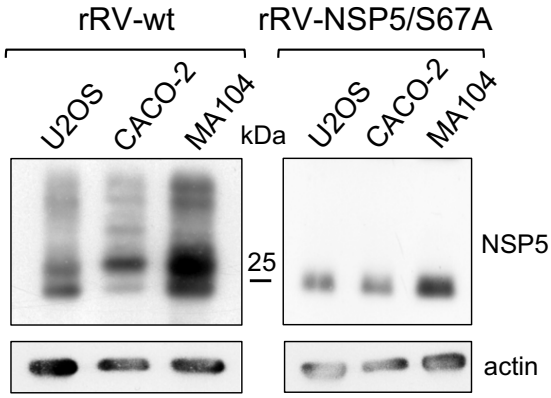

E

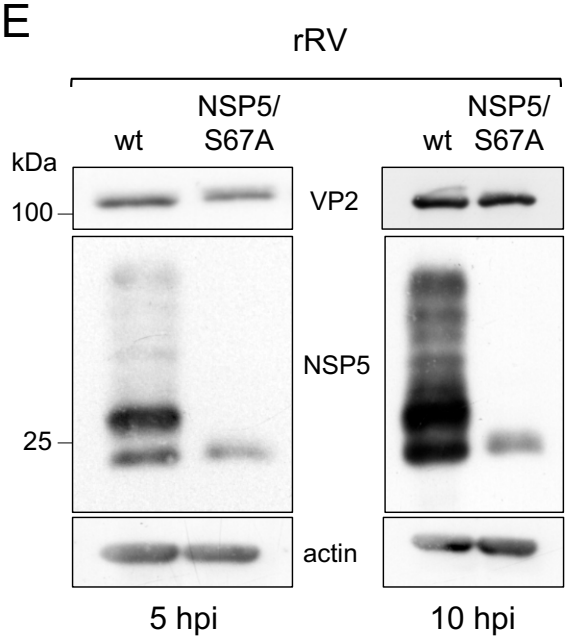

F

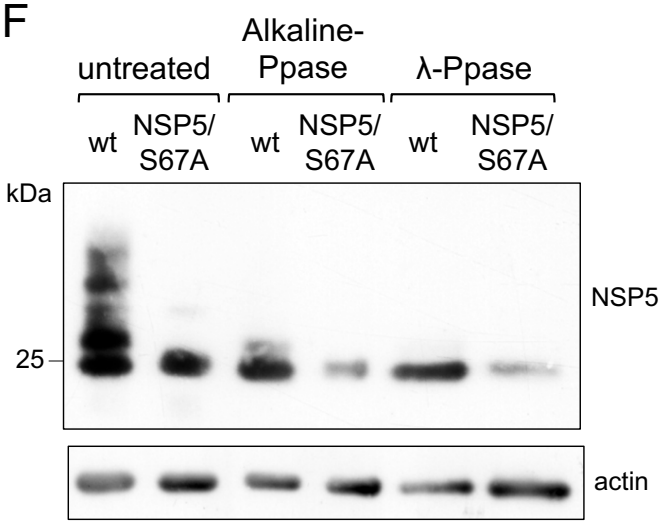

Figure 3

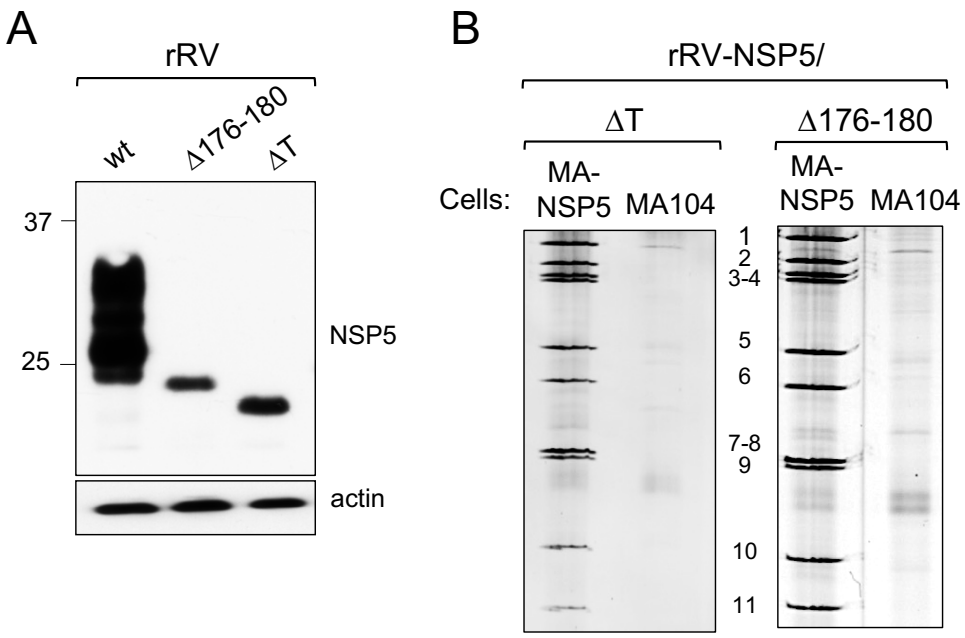
A
rRV
wt
Δ176-180
ΔT
37
25
NSP5
actin
B
rRV-NSP5/
ΔT
Δ176-180
Cells:
MA-NSP5
MA104
MA-NSP5
MA104
1
2
3-4
5
6
7-8
9
10
11

Figure 4

A

rRV-wt

rRV-NSP5/S67A

5 hpi

10 hpi

B

rRV-wt

NSP5

VP6

Merge

rRV-NSP5/S67A

NSP5

VP6

Merge

NSP2

VP6

Merge

VP2

VP6

Merge

C

rRV-NSP5/S67A

NSP5-EGFP

NSP2-mCherry

Figure 4

D

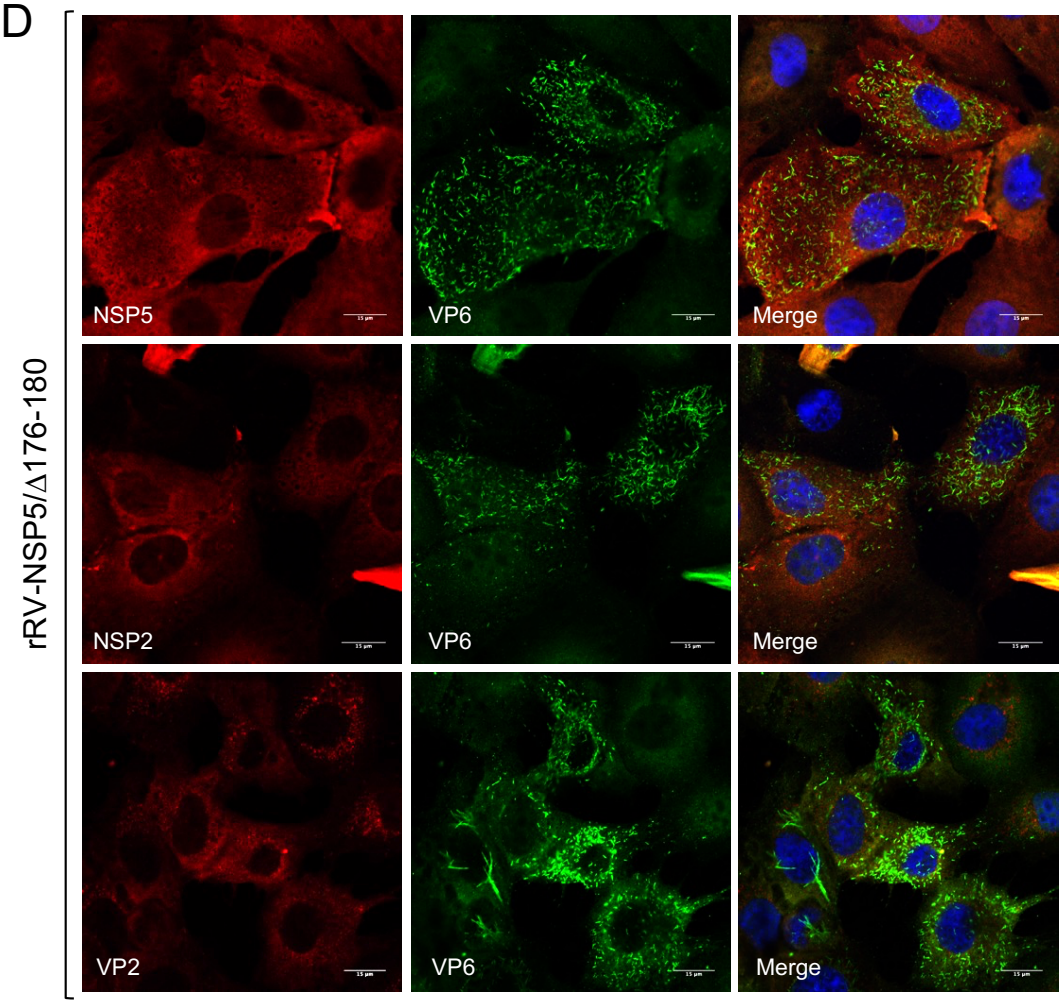
rRV-NSP5/Δ176-180
NSP5
VP6
Merge
NSP2
VP6
Merge
VP2
VP6
Merge

E

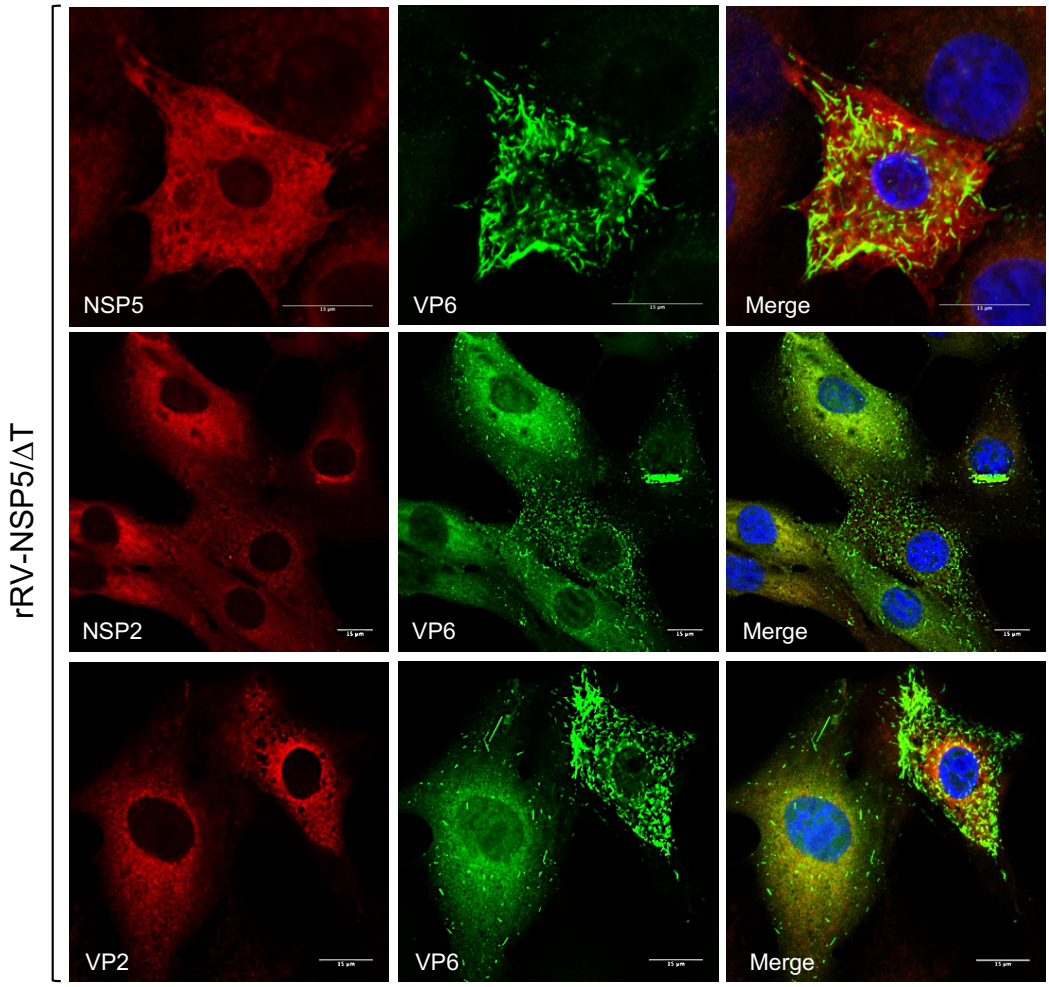
rRV-NSP5/ΔT
NSP5
VP6
Merge
NSP2
VP6
Merge
VP2
VP6
Merge

Figure 5

A

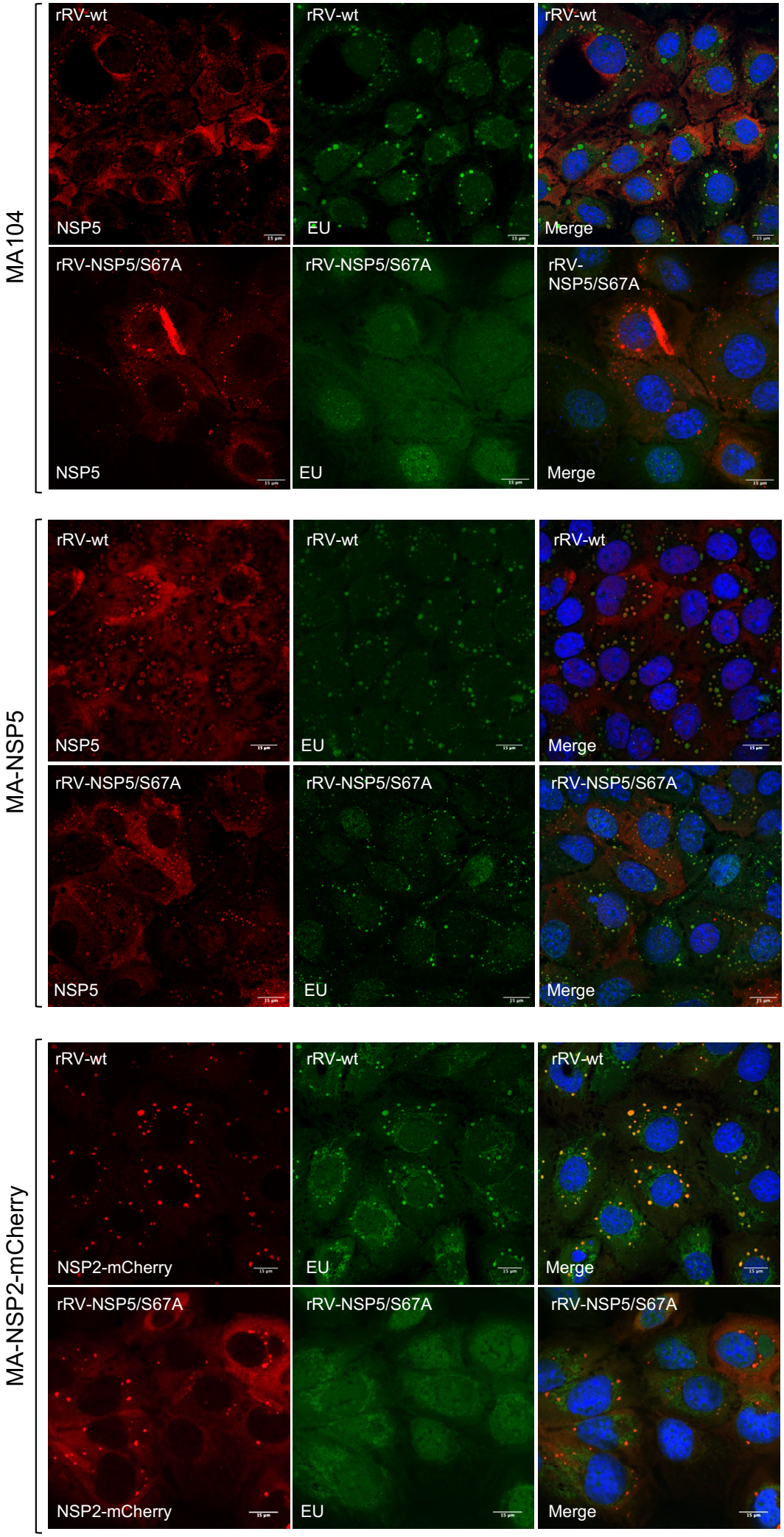
MA104
rRV-wt
NSP5
rRV-wt
EU
rRV-wt
Merge
rRV-NSP5/S67A
NSP5
rRV-NSP5/S67A
EU
rRV-NSP5/S67A
Merge
MA-NSP5
rRV-wt
NSP5
rRV-wt
EU
rRV-wt
Merge
rRV-NSP5/S67A
NSP5
rRV-NSP5/S67A
EU
rRV-NSP5/S67A
Merge
MA-NSP2-mCherry
rRV-wt
NSP2-mCherry
rRV-wt
EU
rRV-wt
Merge
rRV-NSP5/S67A
NSP2-mCherry
rRV-NSP5/S67A
EU
rRV-NSP5/S67A
Merge

Figure 5

B

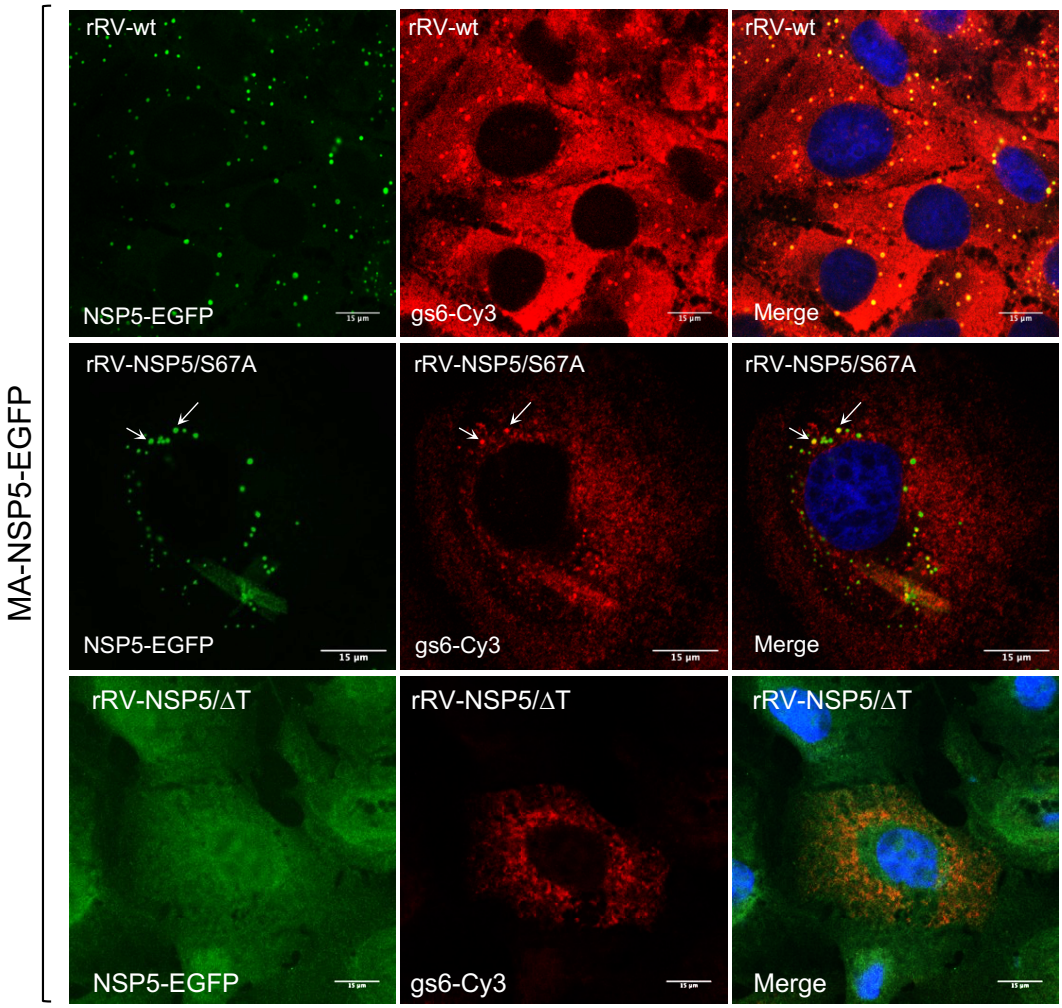
MA-NSP5-EGFP
rRV-wt
NSP5-EGFP
rRV-wt
gs6-Cy3
rRV-wt
Merge
rRV-NSP5/S67A
NSP5-EGFP
rRV-NSP5/S67A
gs6-Cy3
rRV-NSP5/S67A
Merge
rRV-NSP5/ΔT
NSP5-EGFP
rRV-NSP5/ΔT
gs6-Cy3
rRV-NSP5/ΔT
Merge

Figure 6

A

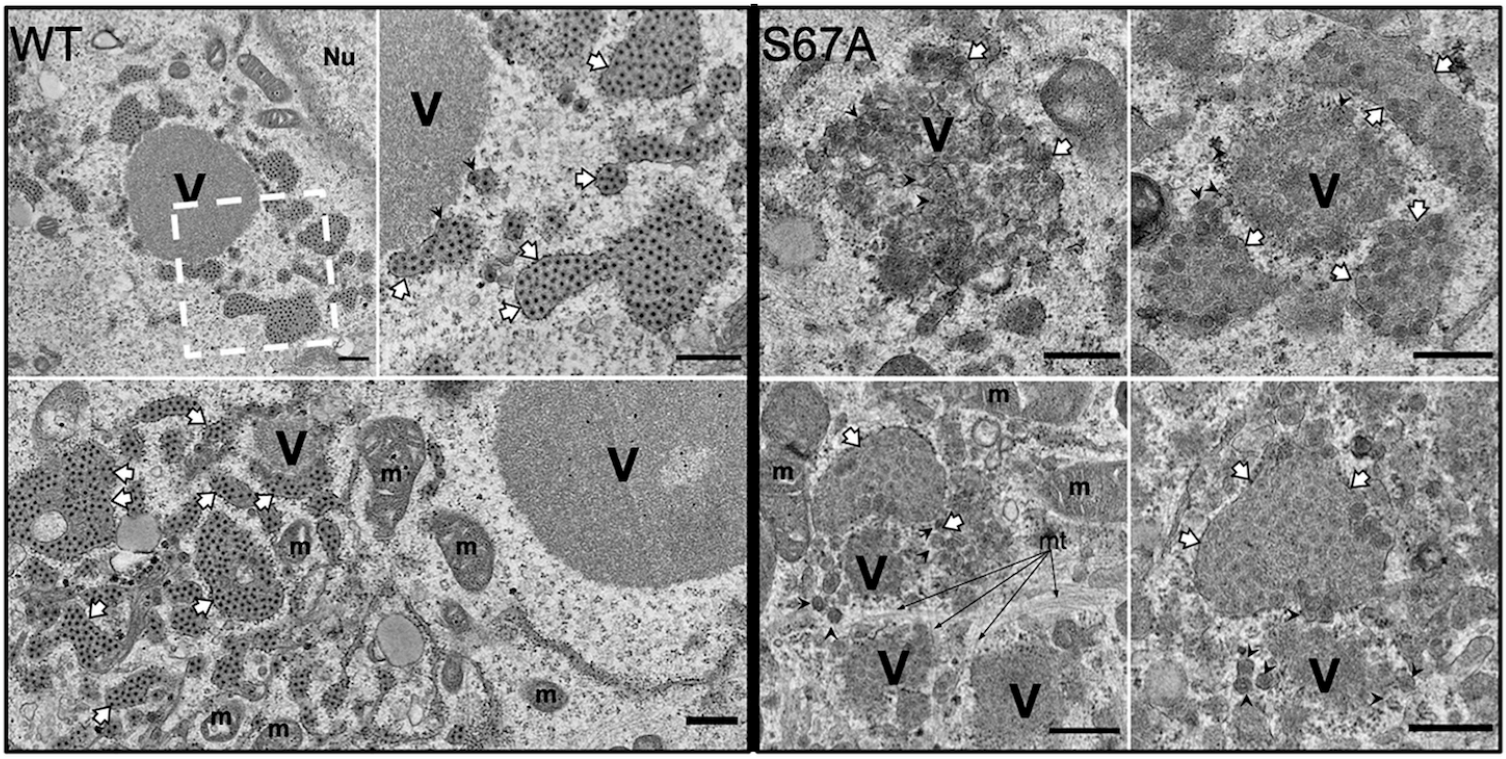
WT
Nu
V
V
V
V
m
m
m
m
m
S67A
V
V
m
m
m
mt
V
V
V
V

B

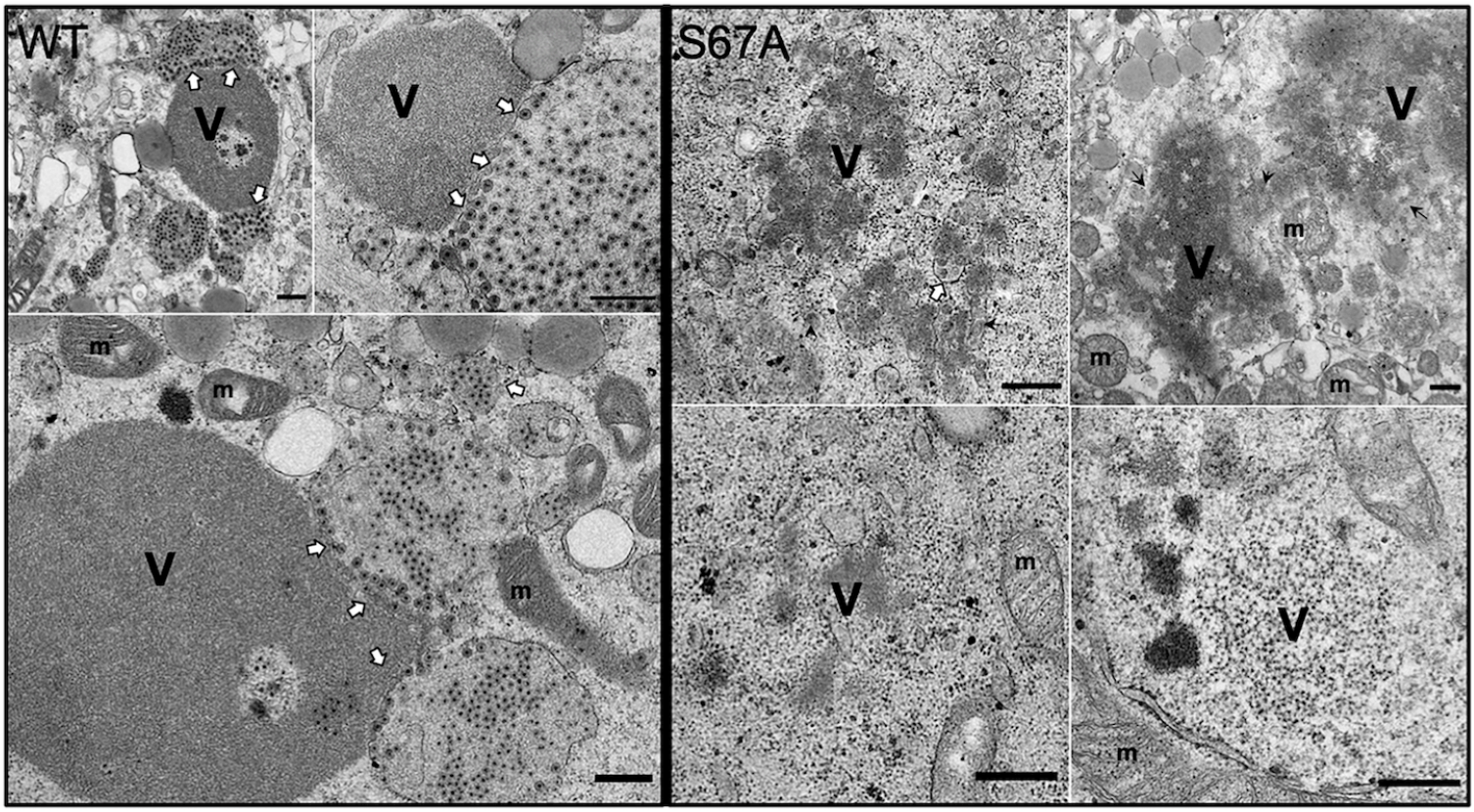
WT
V
V
m
m
V
m
S67A
V
V
m
V
m
m
m
V
V
m

Figure 7

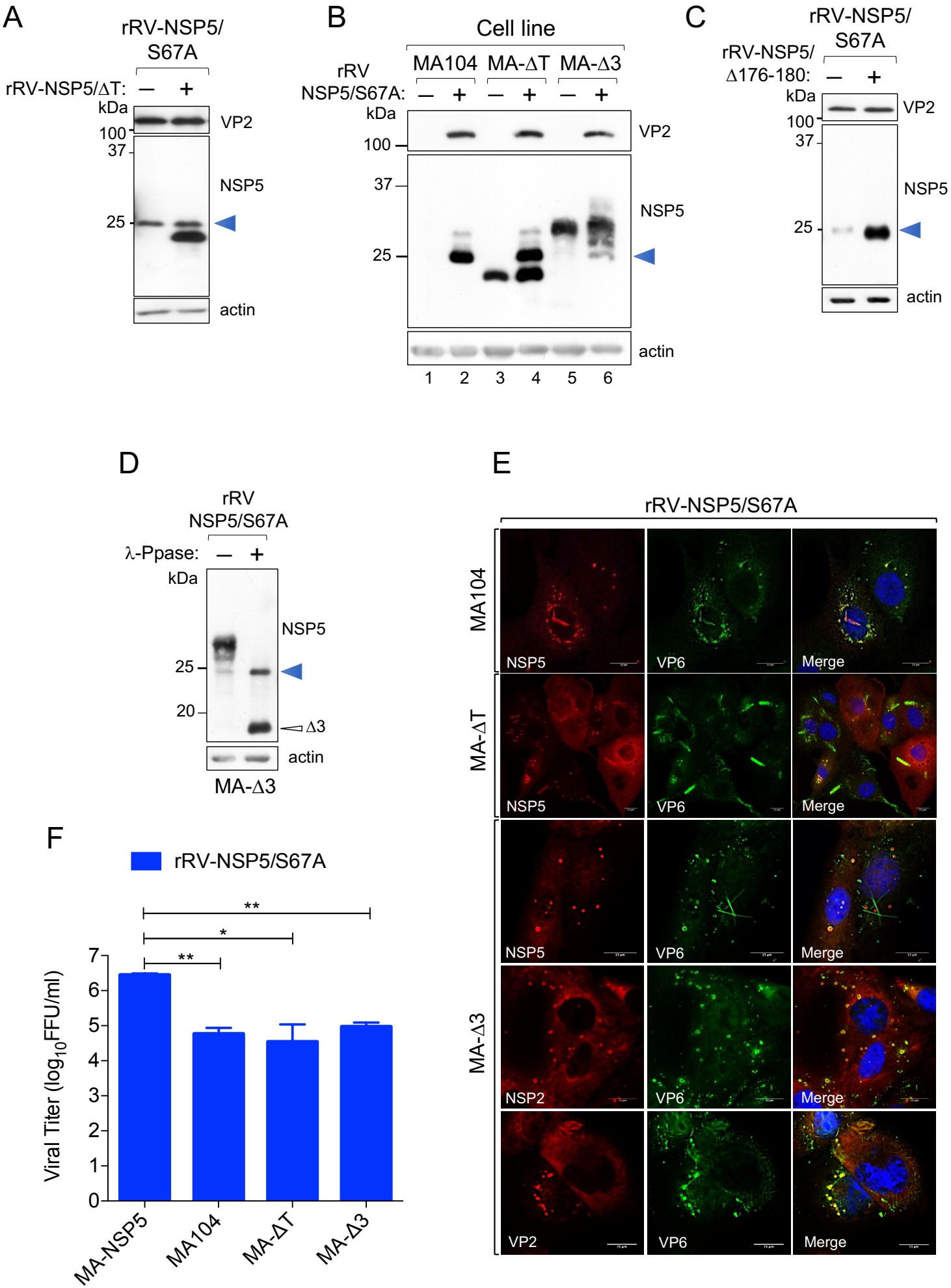
A
rRV-NSP5/S67A
rRV-NSP5/ΔT: — +
kDa
100
37
25
VP2
NSP5
actin
B
Cell line
MA104 MA-ΔT MA-Δ3
rRV NSP5/S67A: — + — + — +
kDa
100
37
25
VP2
NSP5
actin
1 2 3 4 5 6
C
rRV-NSP5/S67A
rRV-NSP5/Δ176-180: — +
kDa
100
37
25
VP2
NSP5
actin
D
rRV NSP5/S67A
λ-Ppase: — +
kDa
25
20
NSP5
Δ3
actin
MA-Δ3
E
rRV-NSP5/S67A
MA104
MA-ΔT
MA-Δ3
NSP5
VP6
Merge
NSP2
VP2
F
rRV-NSP5/S67A
Viral Titer (log10FFU/ml)
0
1
2
3
4
5
6
7
**
*
**
MA-NSP5
MA104
MA-ΔT
MA-Δ3

Figure 8

A

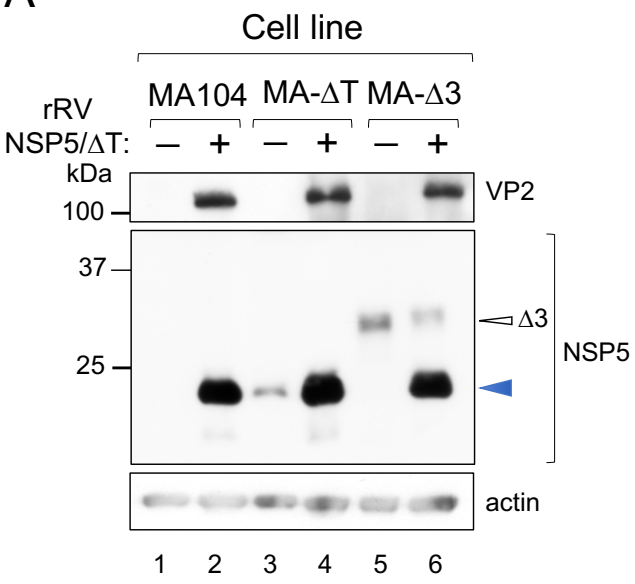

B

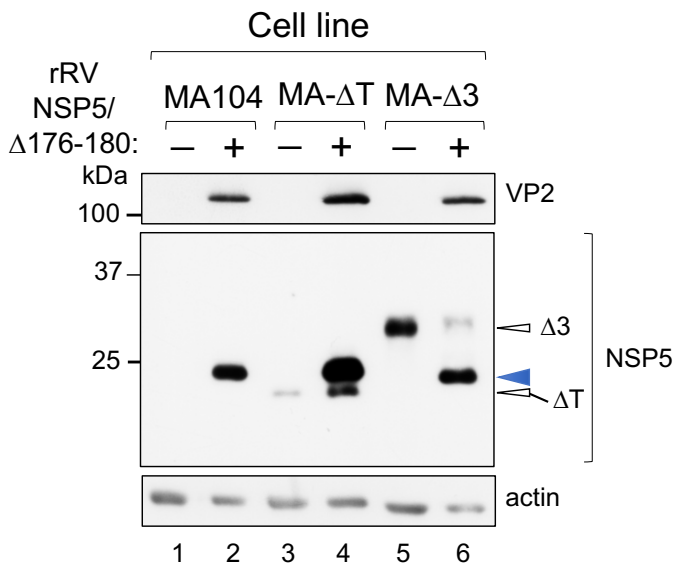

C

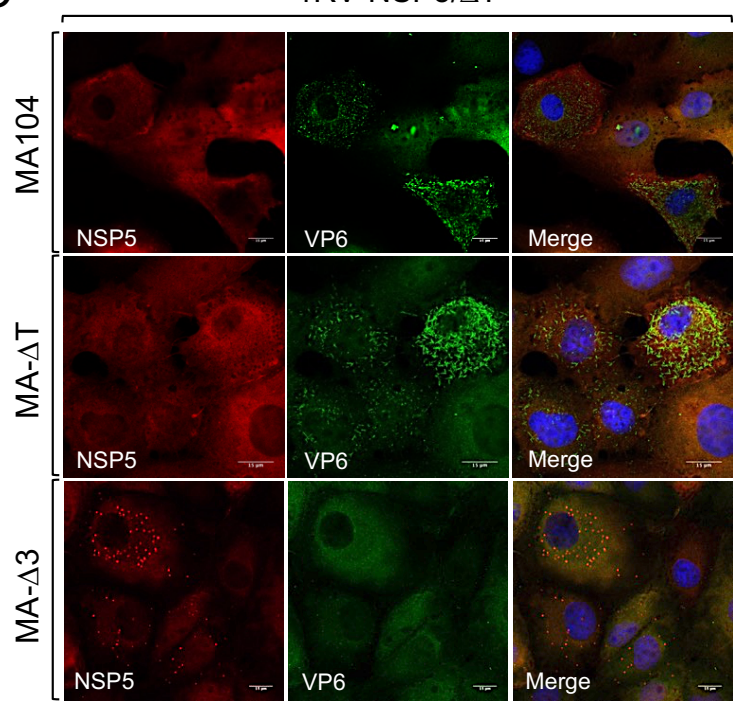

D

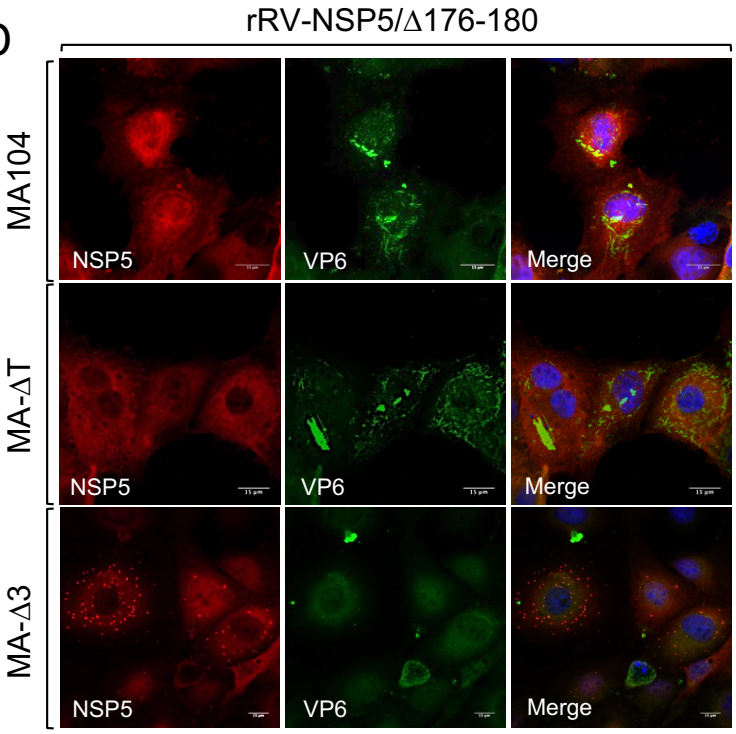

E

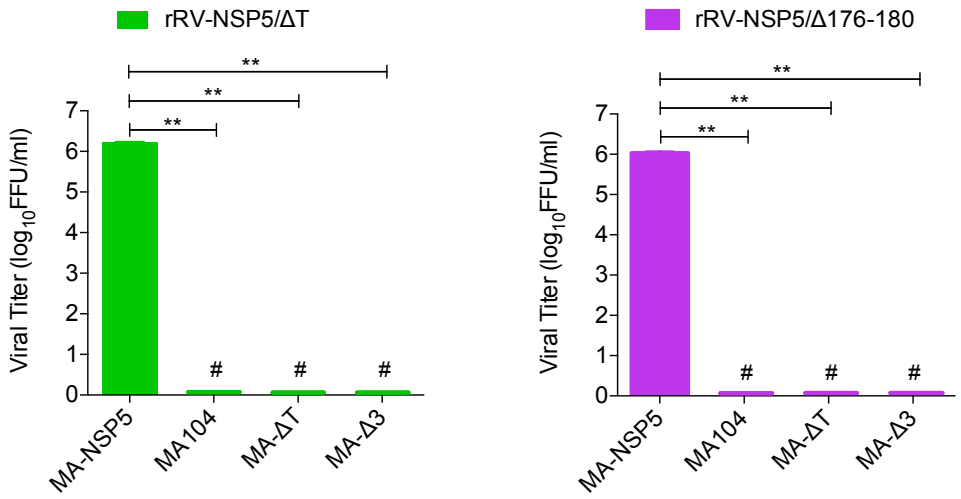

Figure 9

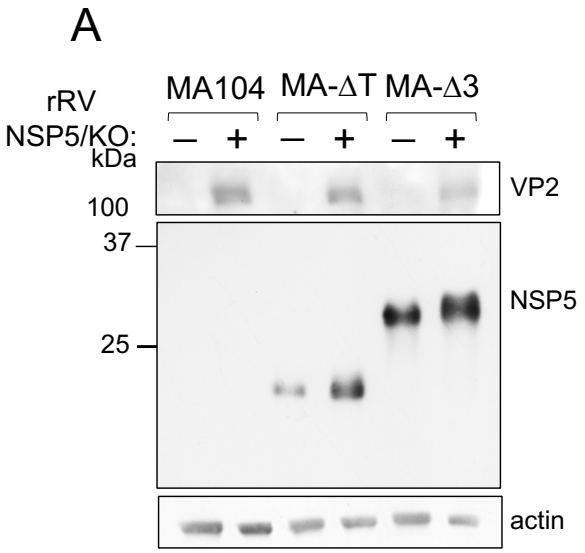
A
rRV
NSP5/KO:
MA104
MA-ΔT
MA-Δ3
– + – + – +
kDa
100
37
25
VP2
NSP5
actin

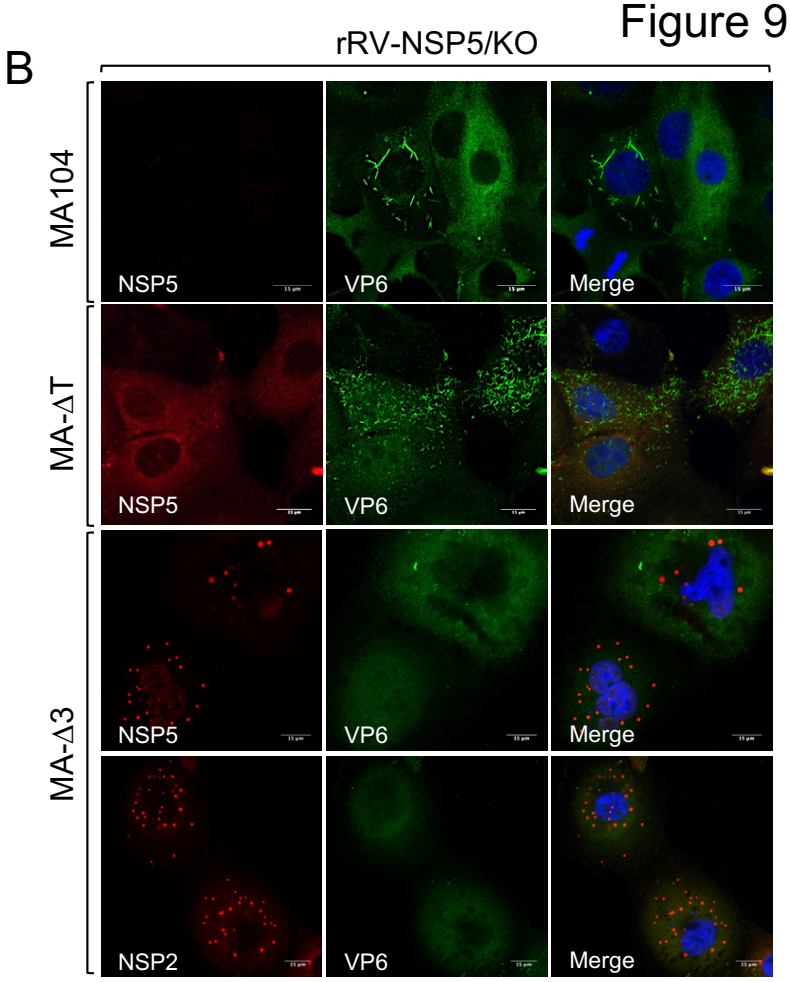
B
rRV-NSP5/KO
MA104
MA-ΔT
MA-Δ3
NSP5
VP6
Merge
NSP2

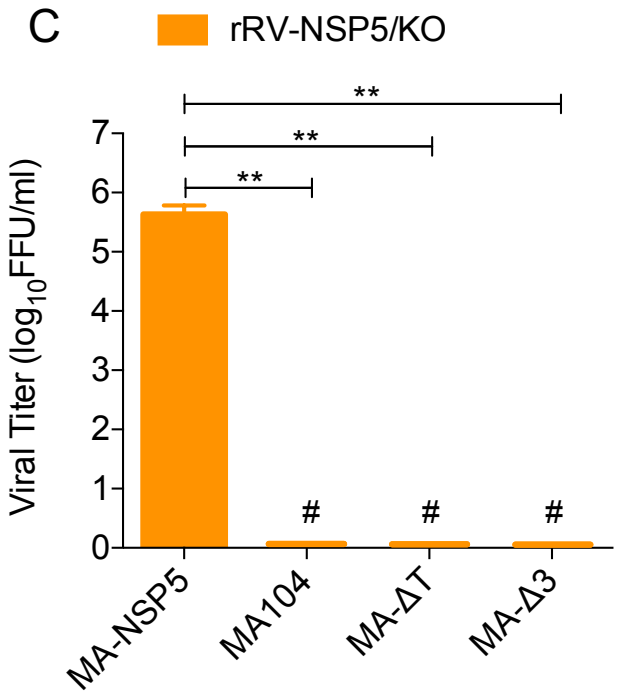
C
rRV-NSP5/KO
Viral Titer (log10FFU/ml)
0
1
2
3
4
5
6
7
**
**
**
#
#
#
MA-NSP5
MA104
MA-ΔT
MA-Δ3

Figure 10

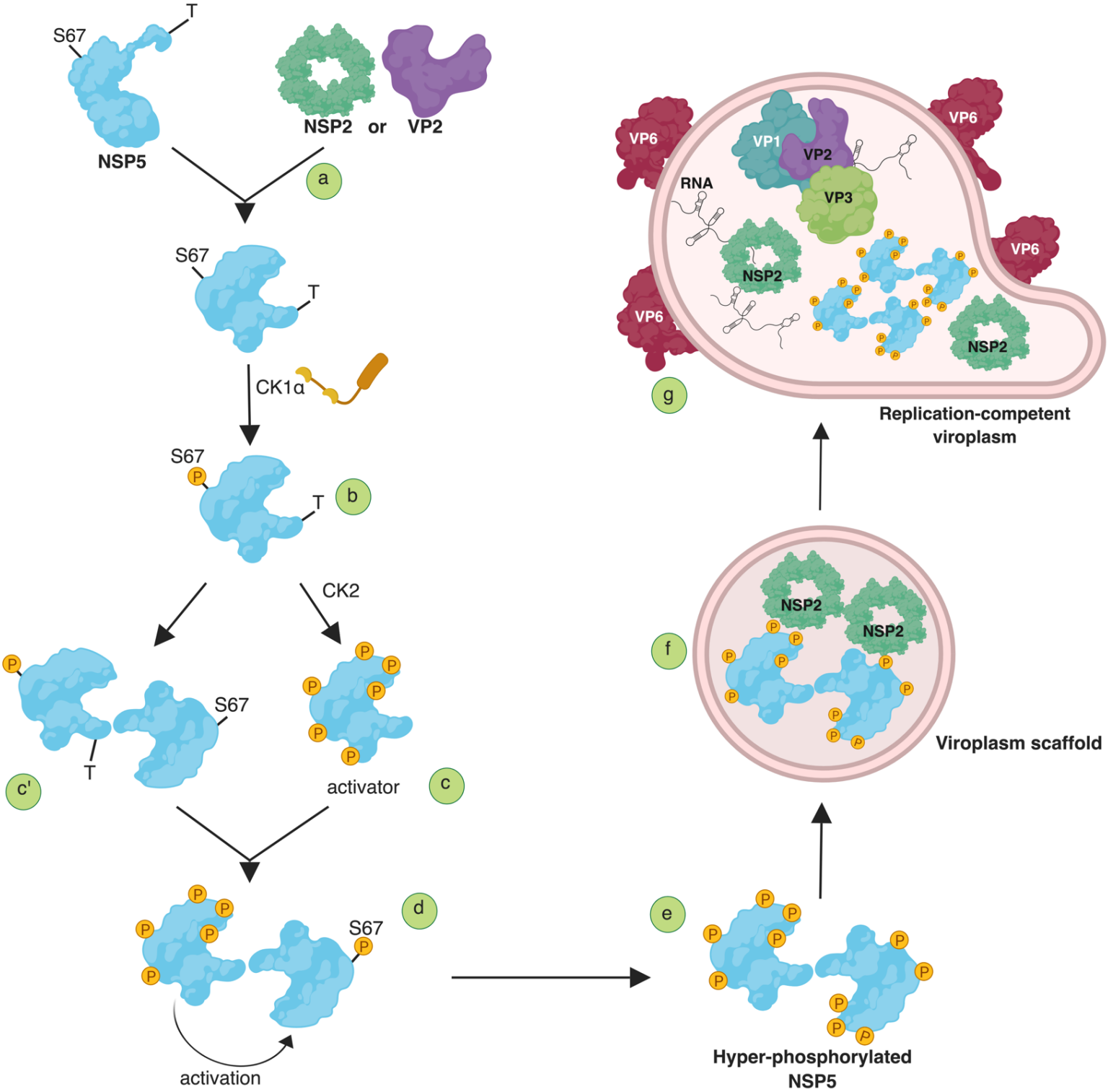
S67
T
NSP5
NSP2 or VP2
a
S67
T
CK1α
S67
P
T
b
CK2
P
S67
T
c'
P
activator
c
P
S67
P
d
activation
e
Hyper-phosphorylated NSP5
f
NSP2
NSP2
Viroplasm scaffold
VP6
VP1
VP2
VP3
RNA
NSP2
NSP2
VP6
VP6
VP6
g
Replication-competent viroplasm